IntechOpen

Bio-Inspired Technology

Edited by Ruby Srivastava
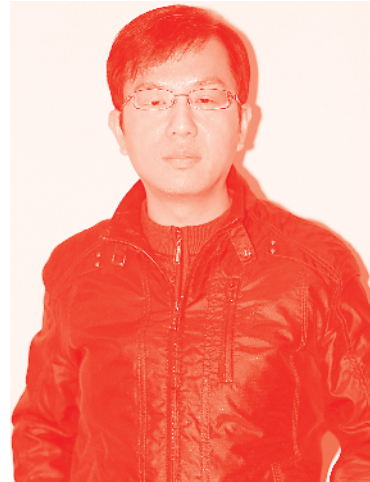
Bio-Inspired Technology

Edited by Ruby Srivastava

IntechOpen

Supporting open minds since 2005

Notice
Statements and opinions expressed in the chapters are these of the individual contributors and not necessarily those of the editors or publisher. No responsibility is accepted for the accuracy of information contained in the published chapters. The publisher assumes no responsibility for any damage or injury to persons or property arising out of the use of any materials, instructions, methods or ideas contained in the book.

We are IntechOpen,
the world's leading publisher of
Open Access books
Built by scientists, for scientists

4,300+
Open access books available

116,000+
International authors and editors

125M+
Downloads

151
Countries delivered to

Our authors are among the
Top 1%
most cited scientists

12.2%
Contributors from top 500 universities

BOOK CITATION INDEX
CLARIVATE ANALYTICS
INDEXED

WEB OF SCIENCE™

Selection of our books indexed in the Book Citation Index
in Web of Science™ Core Collection (BKCI)

Interested in publishing with us?
Contact book.department@intechopen.com

Numbers displayed above are based on latest data collected.
For more information visit www.intechopen.com

Meet the editor

Dr. Ruby Srivastava, a theoretical physicist, is working as a principal investigator on her third project with CSIR-Centre of Cellular and Molecular Biology (CCMB), Hyderabad, under the DST WOS-A scheme. After fifteen years in teaching, she pursued her PhD in 2010 and began her research career with CSIR-Indian Institute of Chemical Technology (IICT). She has published several solo author papers, review articles, seven book chapters, and has served as an editor for many book projects. Her book *Nanostructured Solar Cells* was selected by the Book Citation Index (BKCI) in Web of Science™ Core Collection. One of her journal publications is rated number one among the top 20 papers, and two of her publications have been selected for Longuet-Higgins Early Career Researcher Prizes. She is a reviewer for leading publishing journals and is rated as 0.01% most-read authors by Academia.edu.

Contents

Preface

Nature has always been an inspiring source for humans to mimic devices that are useful for diagnostic and technological applications. Many advanced devices at the nanoscale have been produced with higher accuracy by combining nanotechnology with biology and bioengineering. The book covers the advanced developments of bioactive materials and their broader applications. Chapters provide high-level, technical overviews of the emerging technologies in biological entities for biomedical and electronic applications. It is intended as an introduction to communicate novel research to students, researchers, professionals with technical background, and all readers interested in the applications of nanotechnological devices in a broader perspective.

The book is organized into two sections containing two chapters each:

Section 1: Bioactive Devices for Technological Applications

Section 2: Bioactive Devices for Medical Applications

The book opens with the editor's introductory chapter on DNA as nanowires.

Chapter 2 describes neuromorphic computing, a bioactive device in which neuroscience is transferred to a silicon chip. The authors include the latest developments in the circuit designs of neuromorphic computing and discuss the applicability of their own fabricated spiking neural network chip. The authors conclude the chapter with a discussion of the 3D-IC implementation technique with memristive synapses and the applicability of chaotic time series prediction and video frame recognition.

It has been observed by scientists that the recognition capabilities of DNA and the unique properties of dots and wires can lead to the miniaturization of biological optoelectronic devices as probes and biosensors. As DNA is highly stable and has adjustable conductance, vast information storage, and self-organising capability and programmability, it is considered an ideal candidate for nanodevices, nanoelectronics, and biocomputing. Hence Chapter 2 deals with the device design of nanopillar, nanowall, nanoslit, nanopore structures, nanoball, nanowire, nanoparticles, and quantum dot structures. It also mentions the electrical characterization of DNA-based metallic wires by using transport mechanisms.

Chapter 3 discusses development techniques for new models of hard tissue regeneration using 3D biomaterials inspired by nature. These bioactive materials are a boon to mankind as they can effectively replace infected bone, cartilage, and articular tissues. The authors focus the chapter on porous hydroxyapatite-based ceramic or hybrid scaffolds, which are used in specialized fields such as orthopedics and neurosurgery.

Chapter 4 discusses the various parameters used to support microfluidic disease diagnostics. The authors analyse both theoretical and experimental methods by using the electrical and intrinsic properties of the diseased/infected biological

materials. They emphasise the importance of simulation and modelling techniques and elaborate various applications of dielectrophoresis and electrokinetics. The authors conclude with novel ideas and future electrokinetic methods for detecting diseases at various stages, either with existing diagnostic tools or as independent diagnostic alternatives.

I would like to thank my Author Service Manager Ms. Sandra Maljavac for the continuous support provided during the project. She has been very supportive and helpful to me during this entire journey. *Thank you so much Sandra*. I also wish great success to all my collaborators in their future research activities. It has been a pleasure to collaborate with authors all over the world to contribute to this book.

Ruby Srivastava
CSIR—Centre for Cellular and Molecular Biology,
Hyderabad, India

Section 1

Bioactive Devices for Technological Applications

Chapter 1

Introductory Chapter: DNA as Nanowires

Ruby Srivastava

1. Introduction

The integration of nanotechnology with biology and bioengineering has produced many advances with the manipulation of well-defined structures at the nanoscale with high accuracy. DNA molecules can be used for the assembly of devices, for the interconnect joints, or as the device element itself. Sequence-specific DNA detection has been applied in the diagnosis of pathogenic and genetic diseases. The unique physical properties of dots or wires with the remarkable recognition capabilities of DNA could lead to the miniaturization of biological electronics and optical devices, which includes the biosensors and probes. Numerous advantages of nano- and micro-biodevices include the separation technologies, HPLC and capillary electrophoretic separation of DNA, nanopillar devices for the ultra-fast separation of DNA and proteins, nanoball materials for the fast separation of wide range of DNA fragments and the nanowire devices for ultra-fast separation of DNA, RNA, and proteins. The studies about these devices have been carried out by *Prof. Yoshinobu Baba* and the research group [1–12]. The nanopillar, nanowall, nanoslit, and nanopore structures were designed by the top down or semiconductor nano-fabrication technology, while the nanoball, nanowire, nanoparticles and the quantum dot structures are designed by the use of bottom up or self-assembled nano-fabrication technology. These devices are shown in **Figure 1**.

DNA exhibits many other properties; as high stability, adjustable conductance, vast information storage, self-organising capability and programmability. So it is considered as an ideal material for the applications of nanodevices, nanoelectronics and molecular computing. There are several advantages to use DNA for these device designs. The first step of the DNA-based nanotechnology is to attach DNA molecules to the surfaces. It can be done by three different methods: by electrostatic interaction between DNA and a substrate, covalent binding of a chemical group attached to the DNA end and the binding of protein attached at the DNA end to the corresponding antibody immobilized at the surface. Seeman and co-workers [13] have exploited the properties of DNA's molecular recognition to design complex mesoscopic structures based solely on DNA. They used the branched DNA to form stick figures by properly choosing the sequence of the complementary strands. Further macrocycles, DNA quadrilateral, DNA knots, Holliday junctions, and other periodic crystal structures were also designed. DNA-mediated self-assembly of nanostructures has been extended to metallic nanowires [14–16]. In a study, DNA as a template was used to grow conducting silver nanowires [14]. The fabrication of gold and silver wires was used with the DNA as a template or skeleton [15]. Nguyen et al. developed an approach for the attachment of DNA to oxidatively open the ends of multiwall carbon nanotube arrays [17]. The carbon wall nanotubes can be used as electrodes to transmit electrical signals or as sensors to detect the concentration of chemical or
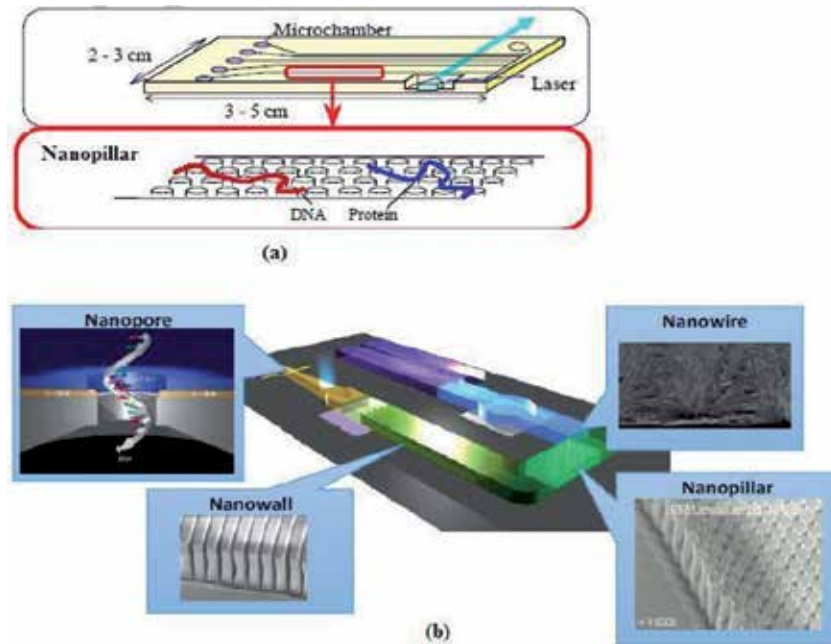
Figure 1.
(a) Device design of nanopillar and (b) nanobiodevices with nanopore, nanopillar, nanowire and nanowell. Adapted from Ref. [1].

biological materials [18–20]. Efficient DNA delivery is vital for the gene therapy, DNA vaccination and the advancement of other clinical therapies. Molecular devices are highly desirable as they can rapidly accumulate and displace electrons/charges within the nanoscale structures, and are sensitive to the changes in the physicochemical and biological environments. DNA logic gates can also constructed from the concepts based on the DNA tweezers [21]. Molecular wires and/or machines resemble electronic memory units can be made by cost-effective and low-energy technologies, so that they can provide the environmental friendly solutions. DNA origami has gained much attention recently because of its potential to direct the formation of predefined 2D or 3D DNA structures at the nanoscale [22].

DNA nanomachines can also be fuelled by enzymes or DNA [23, 24]. An enzyme-operated DNA-switch was proposed recently [24]. DNA-protein conjugates were widely applied in the development of immunoassays, biosensors, micro-chips and molecular devices [25]. A field effect transistor was also designed, based on the DNA base deoxyguanosine derivative [26]. The replacement of the natural bases can be carried out by the artificial nucleosides or nucleoside mimics [27]. Metal ions (Cu^{2+}, Pd^{2+}, and Ag^+) have been successfully incorporated as artificial DNA bases into the oligonucleotides [28]. Ni-DNA nanowires exhibit the characteristics of memristors, find potential application in mass information storage system [12]. The Ni-DNA device structure is given in **Figure 2**.

Assembling the biomolecules and microorganisms into a desired architecture has offered new routes to the fabrication of nanomaterials [29, 30]. DNA nanowires can be used as a template to fabricate functional nanomaterials and as a platform for genetic analysis [31–33]. These nanowires associate with an aqueous solution of DNA molecules, where capillary forces of the solution at a receding meniscus act to stretch and immobilize the molecules on a solid surface [34]. Yet
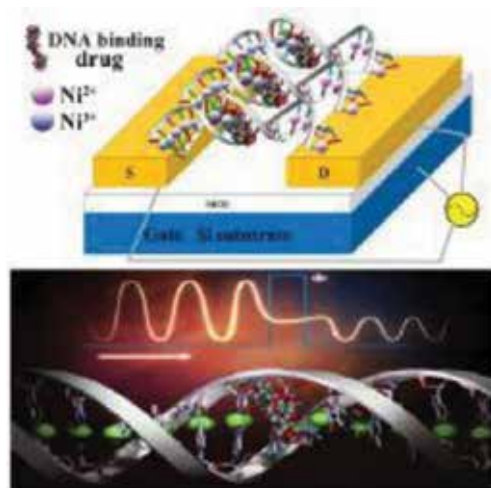
Figure 2.
Ni-DNA nanobiodevice structure. Adapted from Ref. [12].

the widespread use is still hindered due to the limited control over the size, geometry, and alignment of the nanowires. Hence to manipulate the size, geometry, and alignment of nanowires, efforts has been needed to control the evaporation of the solutions by adjusting the experimental parameters, such as: concentration and temperature, or by applying external forces that move the droplets in the desired direction [35–37].

2. Electrical characterization of DNA-based metallic nanowires

Novel conductive DNA-based nanomaterial, DNA-peptide wire composed of a DNA core and a peripheral peptide layer, is used for the wide variety of nano electronic and biosensor applications. The electrical conductivity of these wires is higher than the native double-stranded DNA (dsDNA). These wires produce high conductivity and better resistance to the mechanical deformations caused by the interactions between the substrate and electrode surface. Porath et al. [38] has studied the electrical transport through short (10 nm) dsDNA molecules deposited between platinum nanoelectrodes at different temperatures, confirming the reproducible semiconducting behavior with a gap [39, 40].

Electrical studies indicate that the charge transport in DNA is dominated by holes due to the position of the HOMO (highest occupied molecular orbital) and LUMO (lowest unoccupied molecular orbital) levels of DNA with respect to the Fermi energy of the coinage metal contacts (e.g., Au and Pt), though the photo physical studies indicate the transportation of both hole and electron in DNA [41]. As a result, DNA molecule behaves as a p-type nanowire [42]. The representation of conductive silver nanowires and nanoparticles NPs attached on the DNA origami are given in **Figure 3**.

The charge transport is explained by three main mechanisms: single-step-electron-tunnelling, thermal hopping, and domain hopping [43]. The charge transport in DNA occurs predominantly through the guanine bases due to their lowest electrochemical oxidation potential. When the DNA is absorbed on the surface, the conformations are affected by the van der Waals, electrostatic, and hydrophobic interactions within the substrate. Further the behaviour of DNA is

5
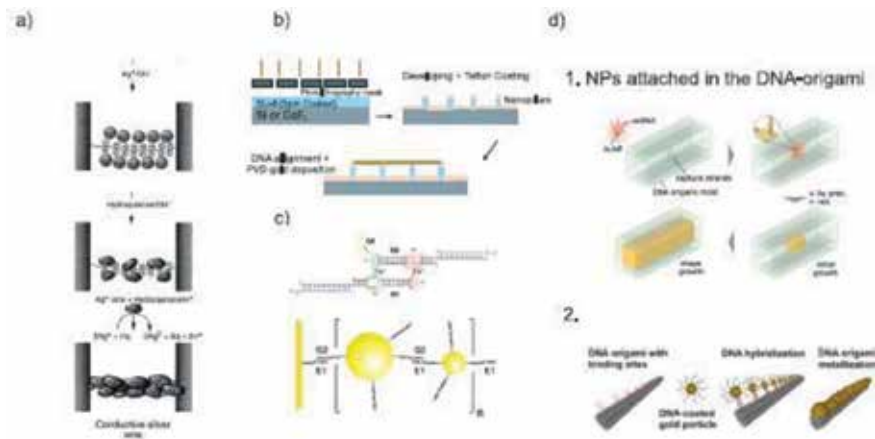
Figure 3.
(a) The construction of conductive silver nanowires, (b) PVD metal deposition on the alignment of DNA NW, (c) RNA functionalized AuNPs and (d) (1) DNA origami molds with Au nanoparticles and (2) nanoparticles NPs attached on the DNA origami. Adapted from Ref. [40].

affected by the DNA sequences, substrate and contact properties, temperature and humidity [44–46]. Recently, studies were conducted on the electrical measurements on guanine quadruplex DNA (G4-DNA), which is uniform in composition, consist of only G-nucleotides and it was observed that G4-DNA exhibit a greater bending rigidity compared to the dsDNA. Several techniques have been developed for contacting the nanowires with the combination of bottom-up and top-down strategies. These are:

a. Lithographically defined contacts and *in situ/ex situ* I–V measurements

b. Conductive AFM measurements

c. DNA Origami-based metal nanostructures

3. Conclusion

DNA acts as a promising material for biomolecular nanotechnology due to its unique recognition capabilities, physicochemical stability, mechanical rigidity and high precision processibility. Significant progress has been made in this field, but it is still in the early stages. The catalytic, electrical, magnetic, and electrochemical properties of such structures can be systematically investigated and will represent the new frontiers in this field. Various DNA-based nanostructures, including DNA itself, DNA functionalized with metal and semiconductor nanoparticles, DNA-directed nanowires, and DNA-functionalized carbon nanotubes are used in wider application for biological and medical applications. Due to the present applicability of DNA structures, these properties should be properly studied to provide an access to the new and useful electronic and photonic materials. The development of DNA nanowires has recently focussed its attention in three aspects: (1) customising the sequence of nucleic acids for better electrical conductivity with reduced mismatch pair complexes, (2) stacking targeted double-helical backbone for stable and rigid nanowires, and (3) interconnection of discrete DNA origami structures [47]. Though researches have been carried out for the achievement of these targets, the cost of experimental synthesis need to be address in near future.

Acknowledgements

Author details

Ruby Srivastava
CSIR—Centre for Cellular and Molecular Biology, Hyderabad, India

*Address all correspondence to: amitruby1@gmail.com

IntechOpen

References

[1] Baba Y. Nano- and microbiodevices for high-performance separation of biomolecules. Chromatography. 2004;**22**:1360-1361. DOI: 10.15583/jpchrom.2015.030

[2] Yasui T, Kaji N, Reza Mohamadi M, Okamoto Y, Tokeshi M, Horiike Y, et al. Electroosmotic flow in microchannels with nanostructures. ACS Nano. 2011;**5**:7775-7780. DOI: 10.1021/nn2030379

[3] Serag MF, Braeckmans K, Habuchi S, Kaji N, Bianco A, Baba Y. Spatiotemporal visualization of subcellular dynamics of carbon nanotubes. Nano Letters. 2012;**12**:6145-6151. DOI: 10.1021/nl3029625

[4] Yasui T, Inoue Y, Naito T, Okamoto Y, Kaji N, Tokeshi M, et al. Inkjet injection of DNA droplets for microchannel array electrophoresis. Analytical Chemistry. 2012;**84**:9282-9286. DOI: 10.1021/ac3020565

[5] Hirano K, Ichikawa M, Ishido T, Ishikawa M, Baba Y, Yoshikawa K. How environmental solution conditions determine the compaction velocity of single DNA molecules. Nucleic Acids Research. 2012;**40**:284-289. DOI: 10.1093/nar/gkr712

[6] Hirano K, Yamamoto YS, Ishido T, Murase N, Ichikawa M, Yoshikawa K, et al. Plasmonic imaging of brownian motion of single DNA molecules spontaneously binding to Ag nanoparticles. Nano Letters. 2013;**13**:1877-1882. DOI: 10.1021/nl304247n

[7] Yasui T, Rahong S, Motoyama K, Yanagida T, Wu Q, Kaji N, et al. DNA manipulation and separation in sublithographic-scale nanowire array. ACS Nano. 2013;**7**:3029-3030. DOI: 10.1021/nn4002424

[8] Rahong S, Yasui T, Yanagida T, Nagashima K, Kanai M, Klamchuen A, et al. Ultrafast and wide range analysis of DNA molecules using rigid network structure of solid nanowires. Scientific Reports. 2014;**4**:5252. DOI: 10.1038/srep05252

[9] Wang J, Aki M, Onoshima D, Arinaga K, Kaji N, Tokeshi M, et al. Electrochemical biosensors: Towards point-of-care cancer diagnostics. Biosensors & Bioelectronics. 2014;**51**:280-285. DOI: 10.1016/j.bios.2013.07.058

[10] Yasaki H, Onoshima D, Yasui T, Yukawa H, Kaji N, Baba Y. Microfluidic transfer of liquid interface for parallel stretching and stamping of terminal-unmodified single DNA molecules in zigzag-shaped microgrooves. Lab on a Chip. 2015;**15**:135-140. DOI: 10.1039/c4lc00990h

[11] Yasui T, Kaji N, Ogawa R, Hashioka S, Tokeshi M, Horiike Y, et al. Arrangement of a nanostructure array to control equilibrium and nonequilibrium transports of macromolecules. Nano Letters. 2015;**15**:3445-3451. DOI: 10.1021/acs.nanolett.5b00783

[12] Pandiana SRK, Yuana CJ, Lina CC, Wanga WH, Changa CC. DNA-based nanowires and nanodevices. Advances in Physics: X. 2017;**2**(1):22-34. DOI: 10.1080/23746149.2016.1254065

[13] Seeman NC. Nucleic acid junctions and lattices. Journal of Theoretical Biology. 1982;**99**:237-247. DOI: 10.1016/0022-5193(82)90002-9

[14] Braun E, Eichen Y, Sivan U, Ben-Yoseph G. DNA-templated assembly and electrode attachment of a conducting silver wire. Nature. 1998;**391**:775-778. DOI: 10.1038/35826

[15] Martin BR, Dermody DJ, Reiss BD, Fang M, Lyon LA, Natan MJ, et al. Orthogonal self-assembly on colloidal gold-platinum nanorods. Advanced Materials. 1999;**11**:1021-1025. DOI: 10.1002/(SICI)1521-4095(199908) 11:12<1021

[16] Guo MX, Neuta IH, Madaboosi N, Nilsson M, and Wijngaart W. Efficient DNA-assisted synthesis of trans-membrane gold nanowires. Microsystems & Nanoengineering. 2018;**4**:17084-17092. DOI: 10.1038/ micronano.2017.84

[17] Nguyen CV, Delzeit L, Cassell AM, Li J, Han J, Meyyappan M. Preparation of nucleic acid functionalized carbon nanotube arrays. Nano Letters. 2002;**2**: 1079-1081. DOI: 10.1021/nl025689f

[18] Abu-Salah KM, Alrokyan SA, Khan MN, Ansari AA. Nanomaterials as analytical tools for genosensors. Sensors. 2010;**10**:963-993. DOI: 10.3390/ s100100963

[19] Behabtu N, Green MJ, Pasquali M. Carbon nanotube-based neat fibers. Nano Today. 2008;**3**(5-6):24-348. DOI: 10.1016/s1748-0132(08)70062-8

[20] Wang J, Lin Y. Functionalized carbon nanotubes and nanofibers for biosensing applications. Trends in Analytical Chemistry. 2008;**27**(7):619-626. DOI: 10.1016/j.trac.2008.05.009

[21] Li XY, Huang J, Jiang H-X, Du Y-C, Han G-M, Kong D-M. Molecular logic gates based on DNA tweezers responsive to multiplex restriction endonucleases. RSC Advances. 2016;**6**:38315-38320. DOI: 10.1039/C6RA05132D

[22] Castro CE, Kilchherr F, Kim DN, Shiao EL, Wauer T, Wortmann P, et al. A primer to scaffolded DNA origami. Nature Methods. 2011;**8**:221-229. DOI: 10.1038/nmeth.1570

[23] Yurke B, Turberfield AJ, Mills AP, Simmel FC, Neumann JL. A DNA-fuelled molecular machine made of DNA. Nature. 2000;**406**:605-608. DOI: 10.1038/35020524

[24] Del Grosso E, Dallaire AM, Vallée-Bélisle A, Ricci F. Enzyme-operated DNA-based nanodevices. Nano Letters. 2015;**15**:8407-8411. DOI: 10.1021/acs. nanolett.5b04566

[25] Niemeyer CM. Chemistry—A European Journal. 2001;7:3189-3195

[26] Maruccio G, Visconti P, Arima V, D'Amico S, Biasco A, D'Amone E, et al. Field effect transistor based on a modified DNA base. Nano Letters. 2003;**3**:479-483. DOI: 10.1021/ nl034046c

[27] Kool ET. Replacing the nucleobases in DNA with designer molecules. Accounts of Chemical Research. 2002;**35**:927-936. DOI: 10.1021/ ar000183u

[28] Wagenknecht H-A. Metal-mediated DNA base pairing and metal arrays in artificial DNA: Towards new nanodevices. Angewandte Chemie, International Edition. 2003;**42**:3204-3206. DOI: 10.1002/anie.200301661

[29] Mao C et al. Virus-based toolkit for the directed synthesis of magnetic and semiconducting nanowires. Science. 2004;**303**:213-217. DOI: 10.1126/ science.1092740

[30] Nguyen K et al. Synthesis of thin and highly conductive DNA-based palladium nanowires. Advanced Materials. 2008;**20**:1099-1104. DOI: 10.1002/adma.200701803

[31] Watson SMD, Pike AR, Pate J, Houlton A, Horrocks BR. DNA-templated nanowires: Morphology and electrical conductivity. Nanoscale. 2014;**6**:4027-4037. DOI: 10.1039/C3NR06767J

[32] Catherall T, Huskisson D, McAdams S, Vijayaraghavan A. Self-assembly of one dimensional DNA-templated structures. Journal of Materials Chemistry C. 2014;**2**:6895-6920. DOI: 10.1039/C4TC00460D

[33] Michalet X et al. Dynamic molecular combing: Stretching the whole human genome for high-resolution studies. Science. 1997;**277**:1518-1523. PMID: 9278517

[34] Bensimon A et al. Alignment and sensitive detection of DNA by a moving interface. Science. 1994;**265**:2096-2098. PMID:7522347

[35] Li B et al. Macroscopic highly aligned DNA nanowires created by controlled evaporative self-assembly. ACS Nano. 2013;**7**:4326-4333. DOI: 10.1021/nn400840y

[36] Li B, Zhang C, Jiang B, Han W, Lin Z. Flow-enabled self-assembly of large-scale aligned nanowires. Angewandte Chemie International Edition in English. 2015;**54**:4250-4254. DOI: 10.1002/anie.201412388

[37] Deen J et al. Combing of genomic DNA from droplets containing picograms of material. ACS Nano. 2015;**9**:809-816. DOI: 10.1021/nn5063497

[38] Porath D, Bezryadin A, de Vries S, Dekker C, De Vries S, Dekker C. Direct measurement of electrical transport through DNA molecules. Nature. 2000;**403**:635-638. DOI: 10.1038/35001029

[39] Cohen H, Nogues C, Naaman R, Porath D. Direct measurement of electrical transport through single DNA molecules of complex sequence. Proceedings of the National Academy of Sciences of the United States of America. 2005;**102**:11589-11593. DOI: 10.1038/35001029

[40] Bayrak T, Jagtap NS, Erbe A. Review of the electrical characterization of

metallic nanowires on DNA templates. International Journal of Molecular Sciences. 2018;**19**:3019-3037. DOI: 10.3390/ijms19103019

[41] Elias B, Shao F, Barton JK. Charge migration along the DNA duplex: Hole versus electron transport. Journal of the American Chemical Society. 2008;**130**:1152-1153. DOI: 10.1021/ja710358p

[42] Takagi S, Takada T, Matsuo N, Yokoyama S, Nakamura M, Yamana K. Gating electrical transport through DNA molecules that bridge between silicon nanogaps. Nanoscale. 2012;**4**:1975-1977. DOI: 10.1039/C2NR12106A

[43] Boon EM, Barton JK. Charge transport in DNA. Current Opinion in Structural Biology. 2002;**12**:320-329. PMID: 12127450

[44] Heim T, Deresmes D, Vuillaume D. Conductivity of DNA probed by conducting-atomic force microscopy: Effects of contact electrode, DNA structure, and surface interactions. Journal of Applied Physics. 2004;**96**:2927-2936. DOI: 10.1063/1.1769606

[45] Dong HH, Nham H, Yoo K-HH, So HM, Lee H-YY, Kawai T. Humidity effects on the conductance of the assembly of DNA molecules. Chemical Physics Letters. 2002;**355**:405-409. DOI: 10.3390/nano7060128

[46] Yamahata C, Collard D, Takekawa T, Kumemura M, Hashiguchi G, Fujita H. Humidity dependence of charge transport through DNA revealed by silicon-based nanotweezers manipulation. Biophysical Journal. 2008;**94**:63-70. DOI: 10.1529/biophysj.107.115980

[47] Eidelshtein G, Kotlyar A, Hashemi M, Gurevich L. Aligned deposition and electrical measurements on single DNA molecules. Nanotechnology. 2015;**26**:475102. DOI: 10.1088/0957-4484/26/47/475102

Opening the "Black Box" of Silicon Chip Design in Neuromorphic Computing

Kangjun Bai and Yang Yi

Abstract

Neuromorphic computing, a bio-inspired computing architecture that transfers neuroscience to silicon chip, has potential to achieve the same level of computation and energy efficiency as mammalian brains. Meanwhile, three-dimensional (3D) integrated circuit (IC) design with non-volatile memory crossbar array uniquely unveils its intrinsic vector-matrix computation with parallel computing capability in neuromorphic computing designs. In this chapter, the state-of-the-art research trend on electronic circuit designs of neuromorphic computing will be introduced. Furthermore, a practical bio-inspired spiking neural network with delay-feedback topology will be discussed. In the endeavor to imitate how human beings process information, our fabricated spiking neural network chip has capability to process analog signal directly, resulting in high energy efficiency with small hardware implementation cost. Mimicking the neurological structure of mammalian brains, the potential of 3D-IC implementation technique with memristive synapses is investigated. Finally, applications on the chaotic time series prediction and the video frame recognition will be demonstrated.

Keywords: analog signal processors, lab on a chip, neuromorphic computing, reservoir computing, analog/mixed-signal circuit design, three-dimensional integrated circuit, image classification

1. Introduction

Benefit by the Moor's law, the von Neumann computing architecture, respectively storing and processing data instructions in the memory unit and the central processing unit (CPU), was served as the major computing model in past several decades [1]. However, physical limitations of the complementary metal-oxide-semiconductor (CMOS) technology and the storage capacity hinder the performance development of classic computers; such classic computers can no longer double its performance every 18 months, indicating the end of Moore's prediction [2].

Recently, the computing efficiency of extracting valuable information in data-intensive applications through the von Neumann computing architecture has become computationally expensive, even with super-computers [3]. The accumulated amount of energy required for the data processing through super-computers poses a query on whether the augmented performance is sustainable.
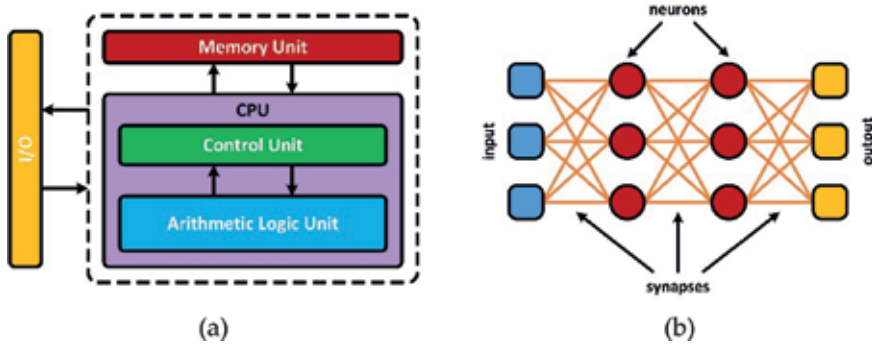
Figure 1.
General architecture of (a) von Neumann computing system and (b) neuromorphic computing system.

As human beings, our brains are capable to analyze and memorize sophisticated information with only $20W$ of energy consumption [4]. In the 1980s, neuromorphic computing, proposed by Dr. Carver Mead, has matured to provide intelligent systems that able to mimic biological processes of mammalian brains through highly parallelized computing architectures; such systems typically model the function of neural network through very-large-scaled-integrated (VLSI) circuits [5]. Major differences between the von Neumann computing architecture and the neuromorphic computing system are illustrated in **Figure 1**. Recently, artificial neural networks (ANNs) have demonstrated their superior performance in many data-extensive applications, including image classification [6–8], handwritten digit recognition [9–11], speech recognition [12, 13] and others. For instance, *TrueNorth*, the neuromorphic chip fabricated by IBM in 2014, is capable to classify multiple objects within a 240×240-pixel video input with merely $65mW$ of energy consumption. Compared to the von Neumann computing system, such a neuromorphic computing system has five orders of magnitude more energy efficient [14]. *Loihi*, the latest prototype of brain-inspired chip fabricated by Intel in 2017, involves a mere 1/1000 power consumption of the one used by a classic computer [15].

Most recent hardware implementations on neuromorphic computing systems focus on the digital computation because of its advantages in noise immunity [16]. However, real-time data information is often recorded in the analog format; thereby, power-hungry operations, such as analog-to-digital (A/D) and digital-to-analog (D/A) conversions, are needed to facilitate the digital computation. It can be observed that the digital computation results in high power consumption with a large design area.

In this chapter, an overview of ANNs will be discussed in Section 2. Section 3 introduces the spiking information processing technique through the temporal code with the leaky integrate-and-fire neuron. Our fabricated spiking neural network chip along with its measurement results on the chaotic behavior will be demonstrated in Section 4, followed by the investigation on 3D-IC implementation technique with memristive synapses in Section 5. Applications on the chaotic time series predication and the image recognition are illustrated in Section 6.

2. Artificial neural networks

In the endeavor to imitate the nervous system within mammalian brains, ANNs are built by employing electronic circuits to imitate biological neural networks [17]. In general, ANN methodologies adopt the biological behavior of neurons and synapses, so-call the hidden layer, in their architecture. The hidden layer is constituted by multiple "neurons" and "synapses", which carries activation functions that

control the propagation of neuron signals. Based on the connection pattern and the learning algorithm, ANN methodologies can be classified into various categories, as depicted in **Figure 2**.

The multilayer perceptron (MLP), a representation of feedforward neural networks (FNNs), is composed by unidirectional connections between hidden layers. MLP has become the quintessential ANN model due to its advantages in ease of implementation [18]. However, the major design challenge in the MLP is that the runtime as well as the training and learning accuracy of the system are strongly affected by the number of neurons and hidden layers. As the neural information evolved into a much more sophisticated mixed-signal evaluation, disadvantages of MLP are exposed when such a neural network is deployed for temporal-spatial information processing tasks [19]. Recurrent neural networks (RNNs), successfully adopt the temporal-spatial characteristics within their hidden layer, closely mimic the working mechanism of biological neurons and synapses. However, the major design challenge is that all weights within the network need to be trained, which dramatically increases its computational complexity. In earlier 2000s, the reservoir computing, an emerging computing paradigm, exploits the dynamic behavior of conventional RNNs and computationally evolved its training mechanism [20]. Within the reservoir layer, synaptic connections are constructed by a layer of nonlinear neurons with fixed and untrained weights. In the reservoir computing, the complexity of the training process is significantly reduced, since only output weights are needed to be trained, thereby, higher computational efficiency can be achieved.

The conventional reservoir computing has been fully developed in the past decade to simplify the training operation of RNNs and proven its benefits across multifaceted applications [21–24]; however, the computational accuracy of the system is still highly proportional to the number of neurons within the reservoir layer. It can be observed that these enormous numbers of neurons significantly hinder the hardware development on the reservoir computing. In [25], it has been proven that the computing architecture is capable to exhibit rich dynamic behaviors during operations when the delay is employed into the system. Benefit from the embedded delay property, the training mechanism and the computing architecture of conventional reservoir computing have conceptually evolved, namely the time delay reservoir (TDR) computing [26]. In the TDR computing, the reservoir layer is built by only one nonlinear neuron with a feedback loop. In this context, time-series input data can be processed through the TDR computing by taking advantages of the feedback signal to form a short-term memory, thereby, higher computational efficiency and accuracy can be achieved.
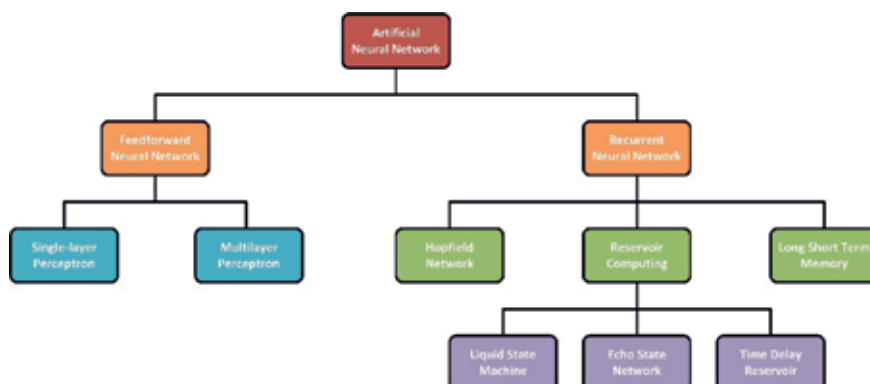
Figure 2.
Overview of artificial neural networks.

3. Spiking information processing

In many brain-inspired neuromorphic computing systems, the interface between modules is often influenced by the signal propagation. The major design challenge in neuromorphic computing is the difficulty in adapting raw analog signals into a suitable data pattern, which can be used in the neuronal activities. Before digging deep into the architecture of our fabricated spiking neural network chip, in this section, a temporal encoding scheme through the analog IC design technique will be discussed.

3.1 CMOS neuron models

In past few decades, researches on biological neurons have been fully investigated in the field of neuroscience [27–32]. In general, the dendrite, the soma, the axon and the synapse are four major elements of a biological neuron [33]. Within a nervous system, dendrites collect and transmit neural signal to the soma, while the soma plays an important role as the CPU to carry out the operation of the nonlinear transformation. Moreover, signals are processed and transmitted in form of a nerve impulse, also known as the spike [34]. During the operation, an output spike is formed when the input stimulus surpasses the threshold level, indicating as the firing process. **Figure 3** demonstrates a typical firing and resting operation in a biological neuron. Synapses along with the axon are then transmitted the spike data patterns to other neurons.

The leaky integrate-and-fire (LIF) neuron model plays an important role in the neuron design to convert raw analog signals into spikes [35]. **Figure 4** depicts the analog electronic circuit model of a LIF neuron. The input excitation, I_{ex}, can be expressed as

$$I_{ex} = C_m \cdot \frac{dV_m}{dt} + I_{leak}, \tag{1}$$

where C_m is the membrane capacitance, $\frac{dV_m}{dt}$ represents the voltage potential across the membrane capacitor over time, and I_{leak} is the leakage current. During the operation, raw analog signals are firstly converted into an excitation current, which will be used to charge up the potential level across the membrane capacitor. When the voltage potential across the membrane capacitor surpasses the threshold level, the circuit fires a spike as its output. Once the firing process is accomplished, the membrane capacitor will be reset to its initial state until the next firing cycle takes
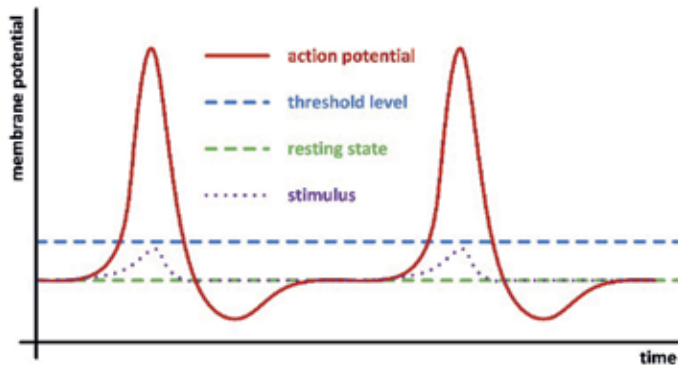
Figure 3.
Action potential of biological impulses.
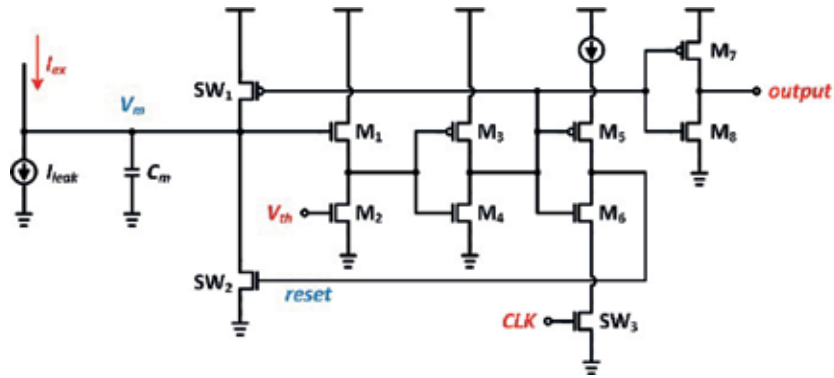
Figure 4.
Analog electronic circuit model of a LIF neuron.

place. The LIF neuron is capable to process both firing and resetting operations, closely mimicking the biological behavior of neurons.

From Eq. (1), it can be observed that the integration time over the membrane capacitor can be regulated by excitation and leakage currents. Such relation can be depicted by a simple resistor model, which can be rewritten as

$$I_{ex} = C_m \cdot \frac{d V_m}{dt} + \frac{V_m}{R_{leak}}, \tag{2}$$

where $\frac{V_m}{R_{leak}}$ determines the amount of leakage current. Thereby, the voltage potential across the membrane capacitor can be determined as

$$V_m = I_{ex} \cdot R_{leak} - e^{\frac{t}{R_{leak} \cdot C_m}}. \tag{3}$$

3.2 Neural codes

Neural code is used to characterize raw analog signals into neural responses. In general, there are two distinct classes to represent neural codes. One class converts analog signals into a spike train where only the number of spikes matters, knowing as the rate code. Another class converts analog signals into the temporal response structure [36] where time intervals matters, knowing as the temporal code.

Figure 5 demonstrates major differences between the rate code and the temporal code. In the rate code, analog signals are encoded into the firing rate within a sampling period, as shown in **Figure 5a**. Considering the implementation complexity, the rate encoding scheme is easier to implement through electronic circuits compared to the temporal encoding scheme; however, small variation of an analog signal in the temporal response structure are neglected, which makes the rate
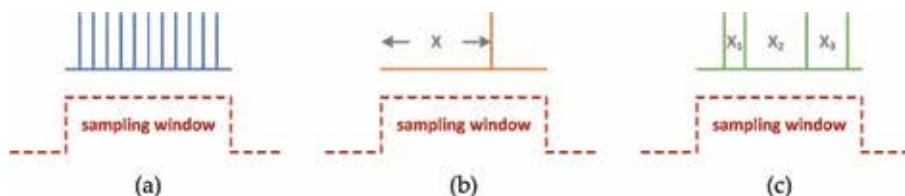
Figure 5.
Neural codes in (a) rate code, (b) time-to-first-spike latency code, and (c) inter-spike-interval temporal code.

code inherency ambiguous in the real-time computation [36]. In [37], researches discover that neural information does not only depend on the spatial, but also the temporal structure. Time-to-first-spike (TTFS) latency code [38–40] is one of the simplest temporal encoding schemes. As demonstrated in **Figure 5b**, in a TTFS latency code, analog signals are encoded into a time interval between the starting point of the sampling period and the generated spike. However, the encoding error would be large if the system performs abnormally.

The inter-spike-interval (ISI) code is another branch of the temporal code, where encoded analog signals depends on the internal time correlation between spikes [41, 42], as illustrated in **Figure 5c**. In general, the ISI temporal encoder converts all analog signals into several inter-spike-intervals, allowing each spike to be the reference frame to others. Obviously, the ISI code is capable of carrying more information within a sampling period compared to the TTFS latency code.

Figure 6a demonstrates the simplified function diagram of ISI temporal encoder. The ISI temporal encoder employs an iteration architecture such that each LIF neuron operates in separate clock periods. The signal regulation layer is built by a current mirror array to duplicate the input excitation current for each LIF neuron; the neuron pool along with the signal integration layer achieve the iterative characteristic. Our ISI temporal encoder chip was fabricated through the standard GlobalFoundries (GF) 180 nm CMOS technology, as depicted in **Figure 6b**.

The number of spikes in an ISI code as discussed in [32] is directly proportional to the number of neurons. Even though this linear proportional correlation is desirable, its hardware implementation is still far more challenging. On the other hand, it can be observed that the exponential relation would increase the number of spikes, thus, containing more information even with the same number of neurons. Through the iterative structured ISI temporal encoder, the number of generated spikes, S_N, can be determined by the number of neurons, which can be written as

$$S_N = 2^N - 1, \tag{4}$$

where N defines the total number of neurons.

From Eq. (4), it can be observed that even with the same number of neurons, the ISI temporal encoder is capable to produce more spikes compared to [35]; thereby,

(a) (b)
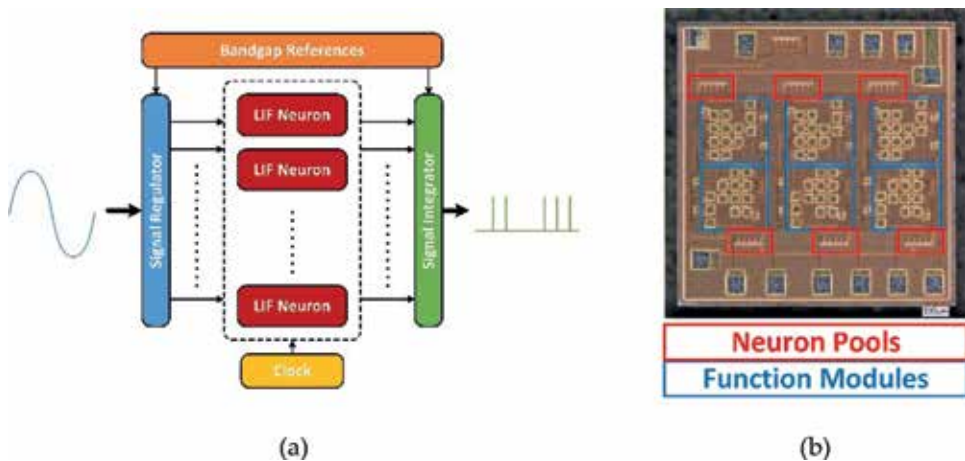
Figure 6.
(a) Simplified function diagram of ISI temporal encoder and (b) die photo of our fabricated ISI temporal encoder chip [32].
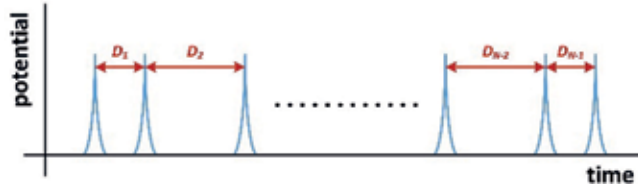
Figure 7.
ISI temporal spike train with N LIF neurons.

the ISI temporal encoder has capability to carry more information. The iterative structure greatly reduces the power consumption, since a smaller number of neurons are needed to produce the equal number of spikes.

In this iterative structured design, the ISI temporal encoder samples the original analog signal without using A/D and D/A conversions, and converts analog signals into several inter-spike-intervals. The expression of the inter-spike-interval can be simplified as

$$D_i = \frac{A_i}{I_{ex} - I_{leak}}, \tag{5}$$

where $A_i = C_m \cdot V_m$. In the IC implementation, the membrane capacitor is fixed, thus, V_i is a constant; thereby, the variable, A_i, in terms of excitation current can be defined as

$$A_i = \beta \cdot A_{N-1} \ = \ \beta^2 \cdot A_{N-2} \ = \ \cdots \ = \beta^{N-1} \cdot A_1, \tag{6}$$

where β is an arbitrary design parameter.

The general expression of each inter-spike-interval, as demonstrated in **Figure 7**, can be written as

$$D_{2^{N-1}-1} = \frac{1}{A_N} \cdot \frac{V_{N-1}}{\beta^{N-1}}, \tag{7}$$

$$D_{2^{N-1}-2} \ = \ \frac{1}{A_1} \cdot \left(\frac{V_{N-2}}{\beta^{N-2}} - \frac{V_{N-1}}{\beta^{N-1}} \right), \tag{8}$$

$$\vdots$$

$$D_{2^{N-1}} = \frac{1}{A_1} \cdot \left(\frac{V_1}{\beta^1} - \frac{V_2}{\beta^2} - \frac{V_3}{\beta^3} - \cdots \ - \frac{V_{N-3}}{\beta^{N-3}} - \frac{V_{N-2}}{\beta^{N-2}} - \frac{V_{N-1}}{\beta^{N-1}} \right). \tag{9}$$

4. CMOS nervous system design

With the respect to the analog design of neural code, our spiking neural network chip adapts the ISI temporal encoding scheme as it pre-signal processing module, as well as the reservoir computing module with delay topology as the processing element. Our spiking neural network, named as the analog delayed feedback reservoir (DFR) system is considered as the simplification of conventional reservoir

computing. By employing the delayed feedback structure within the system, our analog DFR system processes the functionality of high dimensional projection and short-term dynamic memory, whereby the behavior of biological neuron is achieved.

4.1 Architecture of analog DFR system

Figure 8 demonstrates the architecture of our analog DFR system, as published in [43, 44]. During the operation, the high dimensional projection within the reservoir layer, as illustrated in **Figure 9**, is the key module to separate input patterns into different categories [26]. For instance, with low dimensional spaces, two different objects cannot be linearly separated by a single cut-off line, as shown in **Figure 9a**. However, by projecting input patterns onto higher dimensional spaces, from two-dimensional to three-dimensional, the separability of the system changes accordingly. As demonstrated in **Figure 9b**, the same objects are linearly separated by a single cut-off plane without changing their original xy position. Our analog DFR chip was fabricated through the GF 130nm CMOS technology, as demonstrated in **Figure 10**.

In our analog DFR system, the dynamic behavior can be controlled by changing the total delay time within the feedback loop. Along the feedback loop, the total delay time, T, is separated into N intermediate neurons with an identical delayed time constant, τ_{delay}, such that

$$\tau_{delay} = \frac{T}{N}. \tag{10}$$

In the conventional reservoir computing system, represented by the echo state network (ESN), the memory within the reservoir layer fades in time due to the way that neurons are sparsely connected; such fading memory limits the performance of computation [20]. With the delay-feedback topology embedded, our analog DFR system not only reduces the implementation complexity but also overcomes the drawback of fading memory limitation. Such functionality enables the knowledge transfer processing technique, allowing new incoming input data to carry information from its previous states, as depicted in **Figure 11**. The expression of Nth output, S_N, can be simplified as

$$S_N = f\left[I_p(x) + \sum_{x=1}^{N} I_{P-1}(x) \cdot A\,v^x \right], \tag{11}$$

where the function, $f_{[\,]}$, represent the nonlinear transformation of input signal; $I_p(x)$ and $I_{p-1}(x)$ indicate the current and previous input patterns, respectively; Av is the finite gain of the gain regulator within the reservoir layer.

4.2 Delay characteristic

Along the feedback loop, the delay time constant, τ_{delay}, can be controlled by the integration time over the membrane capacitor, which can be expressed as

$$\tau_{delay} = C_m \cdot \frac{V_m}{I_{ex}}. \tag{12}$$

In general, the mathematical model of the delay time constant is represented by the values of resistance and capacitance. In the LIF delay neuron, the input impedance, R_{in}, is equivalent to $\frac{V_m}{I_{ex}}$, thus, the delay time constant can be simplified as

$$\tau_{delay} = C_m \cdot R_{in}. \tag{13}$$

The feedback loop, which is constructed by multiple LIF neurons, as illustrated in **Figure 12**. To enable the spiking signal propagation, the output spike train from the previous neuron is utilized as the clock signal to trigger its following neuron.
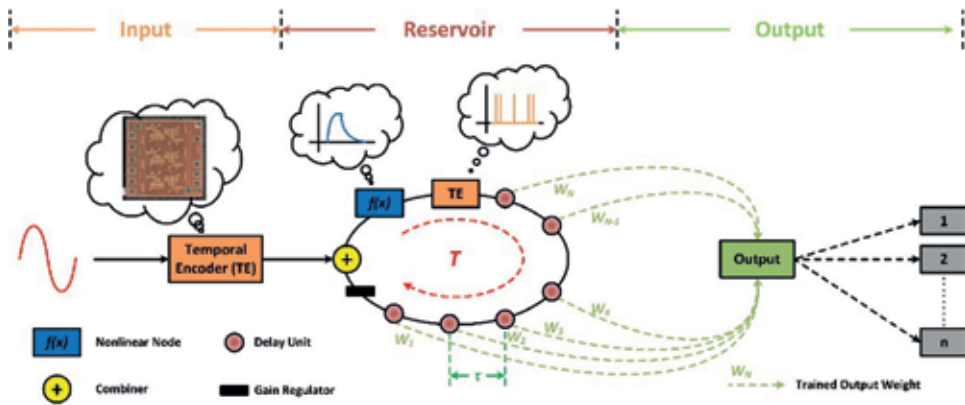
Figure 8.
Architecture of our analog DFR system.
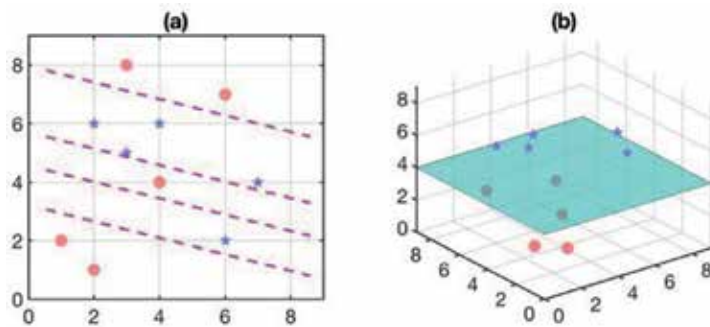
Figure 9.
(a) Nonlinear classification with low dimensional spaces and (b) linear classification with high dimensional spaces.
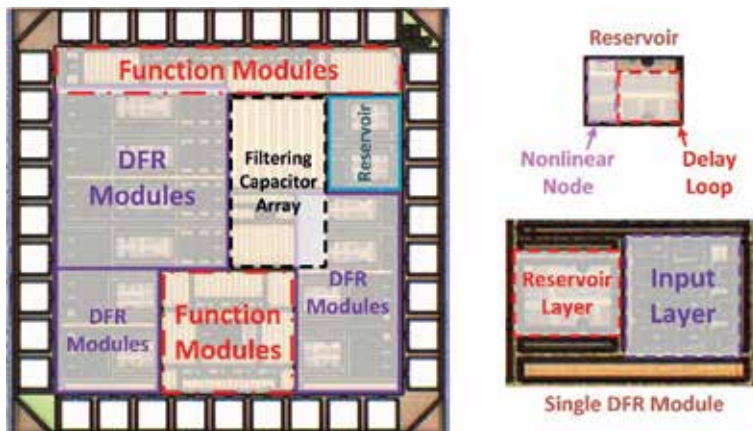
Figure 10.
Die photo of our fabricated analog DFR chip.
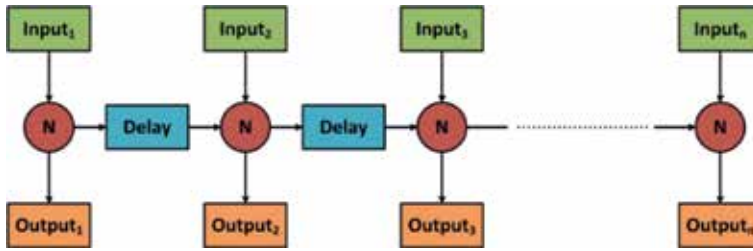
Figure 11.
Illustration of short-term dynamic memory.
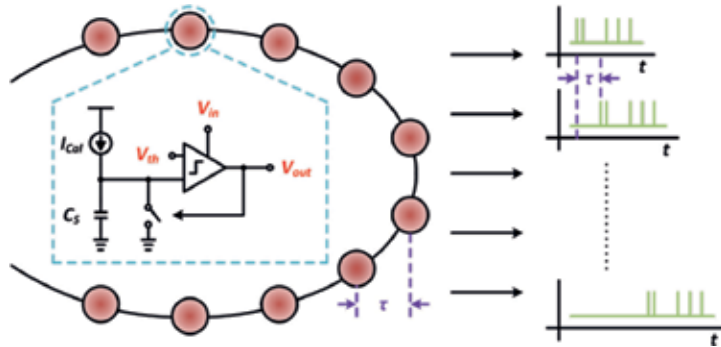
Figure 12.
Dynamic delayed feedback loop.
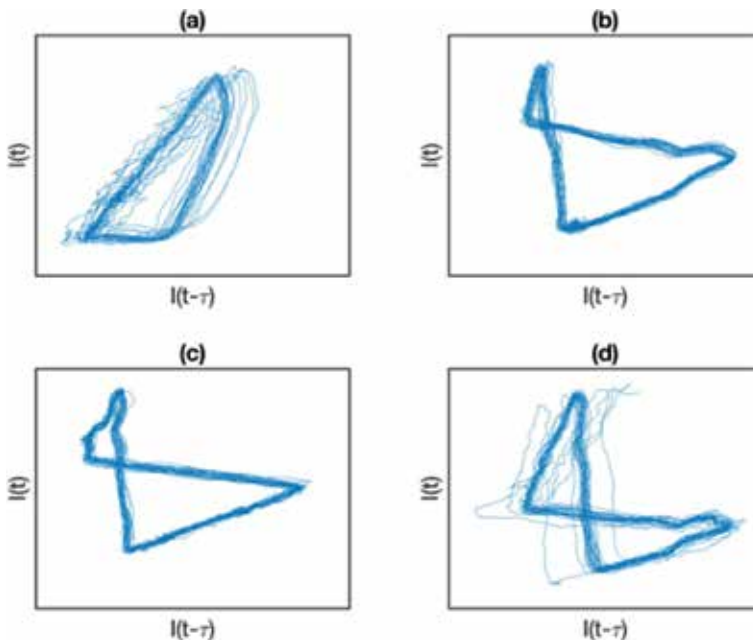
Figure 13.
Measured phase portrait of dynamic system in (a) T = 0.64 μs; *(b)* T = 1 μs; *(c)* T = 1.2 μs; *(d)* T = 1.4 μs.

4.3 Dynamic behavior

In general, the phase portrait is used to visualize how solutions of a delay system would behave. In this experiment, measured phase portraits are plotted through two signals from the feedback loop where one of them is recorded with the time

delay, as shown in **Figure 13**. As the total delay time within the feedback loop increases, the dynamic behavior of the system changes accordingly. As plotted in **Figure 13b**, the delayed signal repeatedly traces its initial path when the total delay time within the feedback loop maintains around 1 μs, indicating as the periodic. When the total delay time within the feedback increases to 1.4 μs, as shown in **Figure 13d**, the delayed signal diverges its initial path but still tracking its equilibrium point, indicating as the edge-of-chaotic.

5. Three-dimensional neuromorphic computing

To closely mimic functionalities of mammalian brains, electronic neurons and synapses in neural network designs need to be constructed in a network configuration, which demands extremely high data communication bandwidth between neurons and high connectivity neural network degree [45, 46]. However, these requirements are not achievable through the traditional von Neumann architecture or the two-dimensional (2D) IC design methodology. Recently, a novel 3D neuromorphic computing system that stacks the neuron and synapse vertically has been proposed as a promising solution with lower power consumption, higher data transferring rate, high network degree, and smaller design area [47, 48]. There are two 3D integration techniques that can be used in the hardware implementation of neuromorphic computing: (1) through-silicon via (TSV) 3D-IC and (2) monolithic 3D-IC. A well-known 3D integration technique is to use the TSV as vertical connection to bond two wafers. In this structure, a large capacitance that is formed by TSVs can be used to build the membrane capacitor, which is required in neuron firing behavior [49–51]. Unlike the TSV 3D-IC technique that uses separately fabrication processes, the monolithic 3D-IC technique is capable to integrate multiple layers of devices at a single wafer, thus, the monolithic 3D-IC technique is capable to provide a smaller design area with lower power consumption [52, 53].

5.1 Memristor

In neural network designs, the electronic circuit model of synapses can be implemented by an emerging non-volatile device, namely the memristor, which is a class of the resistive random-access memory (RRAM). In general, the memristor device is constructed in a metal-insulator-metal (MIM) structure, as illustrated in **Figure 14a**. The resistance of a memristor device can be gradually changed between its low resistance state and high resistance state as the voltage across the memristor device changes.

Memristors are typically fabricated in a 2D crossbar structure [54], which can be further extended to 3D space, as illustrated in **Figure 14c** and **d**, respectively.

5.2 Memristor-based 3D neuromorphic computing

In the field of ANN designs, a novel 3D neural network architecture, which combines memristors and the monolithic 3D-IC technique, has been proposed [55]. In this structure, neurons and memristor-based synaptic array are stacked vertically, as demonstrated in **Figure 15** [48]. As a non-volatile device, RRAM is capable save static power consumption with small implementation area while maintaining its weighted value. With the monolithic 3D-IC technique, the memristor-based 3D neuromorphic computing can potentially reduce the length of critical path by 3X [56], increase the scalability [52], decrease the power consumption by 50% as well as minify the die area by 35% [57].
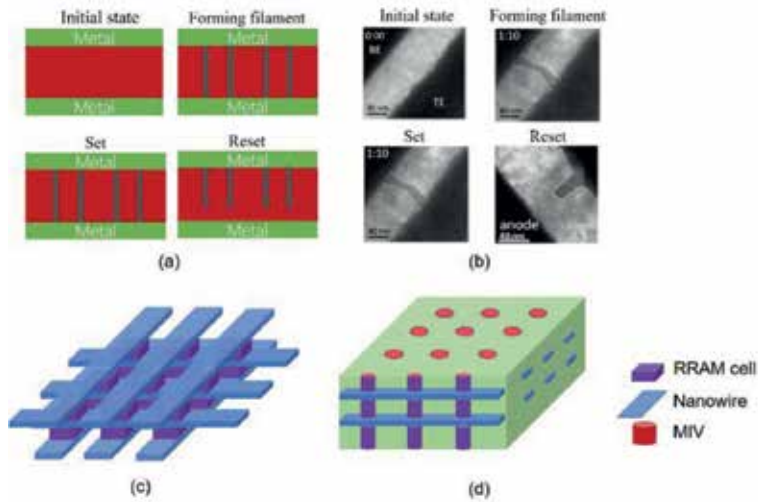
Figure 14.
(a) Switching process of memristor device; (b) transmission electron microscopy images of dynamic evolution of conductive filaments; (c) horizontal RRAM structure; and (d) vertical RRAM structure.
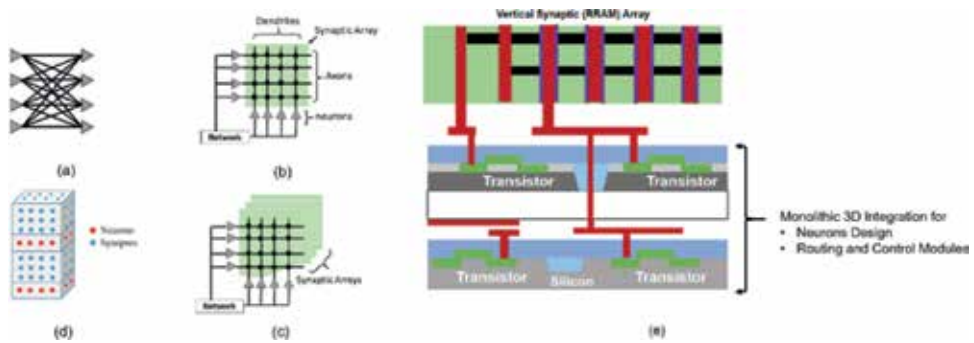
Figure 15.
(a) Typical ANN; (b) 2D structured crossbar array; (c) 3D structured crossbar array; (d) 3D neuromorphic computing architecture by stacking synapses vertically; and (e) deploy monolithic 3D neuromorphic computing on a silicon chip.

6. Lab on a chip

6.1 Chaotic time series prediction

To evaluate the precision of our analog DFR system, a chaotic time series prediction benchmark, the tenth-order nonlinear autoregressive moving average system (NARMA10), is carried out, which can be governed by the following equation

$$O(t) = 0.3 \cdot O(t) + 0.05 \cdot O(t) \cdot \sum_{i=0}^{9} O(t-i) + 1.5 \cdot D(t-9) \qquad (14)$$
$$\cdot D(t) + 0.1,$$

where $D(t)$ is the random input signal at time t, and $O(t)$ is the output signal. In this experiment, 10,000 sampling points were generated through Eq. (14) for training and testing phases. 6000 samples were used for the training while rest samples were used for the testing. The prediction error was then examined through the normalized root mean square error (NRMSE).

In the training phase, output weights were trained by minimizing the deviation between target and predicted outputs. Both training and testing errors were achieved by the NRMSE, which can be defined as

$$NRMSE = \sqrt{\frac{\sum_{i=1}^{N}(y_i - \hat{y}_i)^2}{N\sigma_{\hat{y}}^2}},\qquad(15)$$

where y_i defines the predicted output, $\hat{y}_i$ is the target output, N is the number of samples, and $\sigma_{\hat{y}}^2$ determines the output variance. Experimental results of predicted output signals against target outputs with our analog DFR computing system is plotted in **Figure 16**. From experimental results, the training and testing errors are found to be 8.49 and 6.83%, respectively.

6.2 Video frame recognition

In this task, the application of video frame recognition is chosen to examine the performance of our analog DFR system. In this experiment, 48 images, which comprise three different persons with various face angles, were drawn from the Head Pose Image dataset [58], as demonstrated in **Figure 17a**. Twenty images were used for the training, while another 24 images were used for the testing. In the training phase, the face angle changes from 0 to 75° horizontally. In the testing phase, the rotational angle of face follows the training phase but with additional 15° applied vertically.

As illustrated in Section 4.3, our fabricated analog DFR chip is capable to operate at the edge-of-chaos region as the delay changes. To demonstrate the importance of delay, our model was evaluated through several delayed time constants. As depicted in **Figure 18**, it can be observed that the recognition rate changes with regard to the delay time. For instance, the recognition rate maintains above 98% when the system operates at the edge-of-chaos regime (T = 20 ms) with 10% or less salt-and-pepper noise. As the noise level approaches to 50%, the recognition rate still maintains above 93%. However, if the dynamic behavior of the system deviates from the edge-of-chaos regime, the recognition rate significantly reduces due to the change in the dynamic behavior.
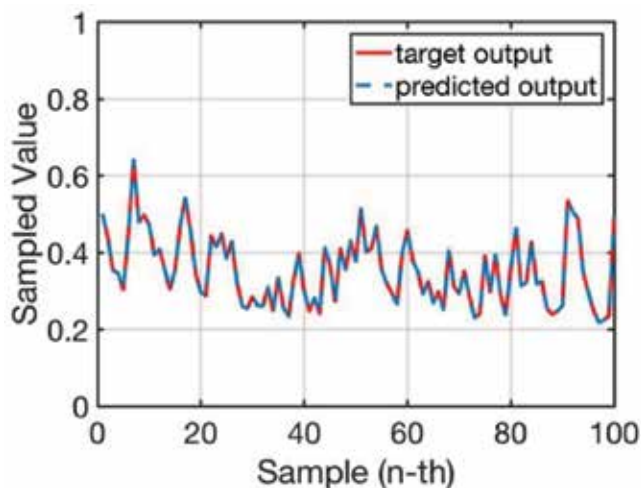
Figure 16.
Target signals versus predicted signals for NARMA10 benchmark.
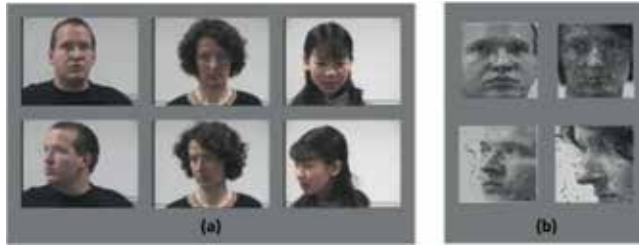
Figure 17.
(a) Training database with three subjects and (b) testing dataset with various salt-and-pepper noise levels.
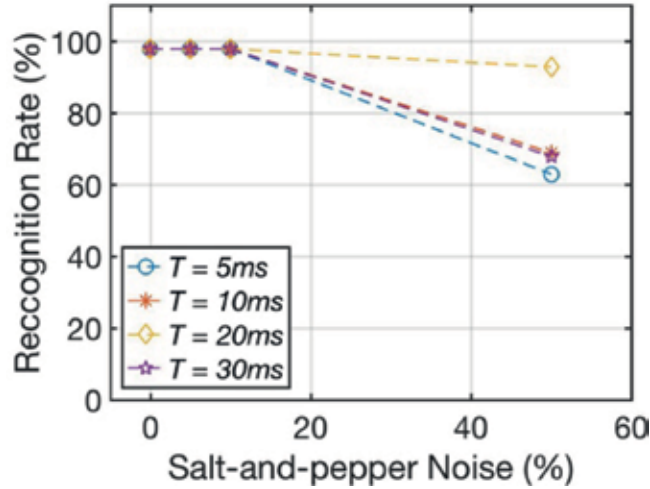
Figure 18.
Recognition rate with respect to various dynamic behavior.

7. Conclusions

In this chapter, the design aspect of our analog DFR system with the analogue electronic circuit model of biological neuron is discussed. By mimicking how human beings process information, our analog DFR system adapts the spiking temporal information processing technique and a nonlinear activation function to project input patterns onto higher dimensional spaces. From measurement results, our analog DFR system demonstrates richness in dynamic behaviors, closely mimicking the biological neurons with delay property. By naturally perform these neuron-like operations, our analog DFR system is capable to nonlinearly project input patterns onto higher dimensional spaces for the classification while operating at the edge-of-chaos region with merely 526 μW of power consumption. Experimental results on the chaotic time series prediction and the video frame recognition demonstrate the high recognition accuracy even with noise, making our analog DFR system a candidate for low power intelligence applications.

Author details

Kangjun Bai and Yang Yi*
The Bradley Department of Electrical and Computer Engineering, Virginia
Polytechnic Institute and State University, Blacksburg, Virginia, USA

*Address all correspondence to: yangyi8@vt.edu

IntechOpen

References

[1] Von Neumann J. The Computer and the Brain. New Haven, USA: Yale University Press; 2012

[2] Schaller RR. Moore's law: Past, present and future. IEEE Spectrum. 1997;**34**(6):52-59

[3] Dayarathna M, Wen Y, Fan R. Data center energy consumption modeling: A survey. IEEE Communication Surveys and Tutorials. 2016;**18**(1):732-794

[4] Yu S et al. An electronic synapse device based on metal oxide resistive switching memory for neuromorphic computation. IEEE Transactions on Electron Devices. 2011;**58**(8):2729-2737

[5] Mead C. Neuromorphic electronic systems. Proceedings of the IEEE. 1990;**78**(10):1629-1636

[6] Krizhevsky A, Sutskever I, Hinton GE. Imagenet classification with deep convolutional neural networks. In: Advances in Neural Information Processing Systems (NIPS). 2012. pp. 1097-1105

[7] Jia Y et al. Caffe: Convolutional architecture for fast feature embedding. In: Proceedings of the 22nd ACM international conference on Multimedia. Florida, USA: ACM; 2014

[8] Simonyan K, Zisserman A. Very deep convolutional networks for large-scale image recognition. arXiv preprint arXiv:1409.1556; 2014

[9] LeCun Y et al. Handwritten digit recognition with a back-propagation network. In: Advances in Neural Information Processing Systems (NIPS). 1990. pp. 396-404

[10] Bottou L et al. Comparison of classifier methods: A case study in handwritten digit recognition. In: IEEE Proceedings of the 12th IAPR International. Conference on Pattern Recognition, 1994. Vol. 2. Conference B: Computer Vision & Image Processing. 1994

[11] Cireşan DC et al. Deep, big, simple neural nets for handwritten digit recognition. Neural Computation. 2010;**22**(12):3207-3220

[12] Hinton G et al. Deep neural networks for acoustic modeling in speech recognition: The shared views of four research groups. IEEE Signal Processing Magazine. 2012;**29**(6):82-97

[13] Mikolov T et al. Strategies for training large scale neural network language models. In: 2011 IEEE Workshop on Automatic Speech Recognition and Understanding (ASRU). Hilton Waikoloa Village, Waikoloa Village, HI: IEEE; 2011

[14] Merolla PA et al. A million spiking-neuron integrated circuit with a scalable communication network and interface. Science. 2014;**345**(6197):668-673

[15] Davies M et al. Loihi: A neuromorphic manycore processor with on-chip learning. IEEE Micro. 2018;**38**(1):82-99

[16] Eryilmaz SB et al. Neuromorphic architectures with electronic synapses. In: 2016 17th International Symposium on Quality Electronic Design (ISQED). Santa Clara, CA, USA: IEEE; 2016

[17] Yegnanarayana B. Artificial Neural Networks. New Delhi, India: PHI Learning Pvt. Ltd.; 2009

[18] LeCun Y, Bengio Y, Hinton G. Deep learning. Nature. 2015;**521**(7553):436

[19] Koch C, Segev I. The role of single neurons in information processing. Nature Neuroscience. 2000;**3**(11s):1171

[20] Jaeger H. Echo state network. Scholarpedia. 2007;**2**(9):2330

[21] Lin X, Yang Z, Song Y. Intelligent stock trading system based on improved technical analysis and Echo State Network. Expert Systems with Applications. 2011;**38**(9):11347-11354

[22] Skowronski MD, Harris JG. Automatic speech recognition using a predictive echo state network classifier. Neural Networks. 2007;**20**(3):414-423

[23] Wang Q, Li Y, Li P. Liquid state machine based pattern recognition on FPGA with firing-activity dependent power gating and approximate computing. In: 2016 IEEE International Symposium on Circuits and Systems (ISCAS). Montreal, Canada: IEEE; 2016

[24] Zhang Y et al. A digital liquid state machine with biologically inspired learning and its application to speech recognition. IEEE Transactions on Neural Networks and Learning Systems. 2015;**26**(11):2635-2649

[25] Legenstein R, Maass W. Edge of chaos and prediction of computational performance for neural circuit models. Neural Networks. 2007;**20**(3):323-334

[26] Appeltant L et al. Information processing using a single dynamical node as complex system. Nature Communications. 2011;**2**:468

[27] Hodgkin AL, Huxley AF. A quantitative description of membrane current and its application to conduction and excitation in nerve. The Journal of Physiology. 1952;**117**(4):500-544

[28] FitzHugh R. Impulses and physiological states in theoretical models of nerve membrane. Biophysical Journal. 1961;**1**(6):445-466

[29] Abbott LF. Lapicque's introduction of the integrate-and-fire model neuron

(1907). Brain Research Bulletin. 1999;**50**(5-6):303-304

[30] Liu Y-H, Wang X-J. Spike-frequency adaptation of a generalized leaky integrate-and-fire model neuron. Journal of Computational Neuroscience. 2001;**10**(1):25-45

[31] Zhao C et al. Neuromorphic encoding system design with chaos based CMOS analog neuron. In: 2015 IEEE Symposium on Computational Intelligence for Security and Defense Applications (CISDA). Verona, NY, USA: IEEE; 2015

[32] Zhao C et al. Interspike-interval-based analog spike-time-dependent encoder for neuromorphic processors. IEEE Transactions on Very Large Scale Integration (VLSI) Systems. 2017;**25**(8):2193-2205

[33] Spruston N. Pyramidal neurons: Dendritic structure and synaptic integration. Nature Reviews Neuroscience. 2008;**9**(3):206

[34] Gerstner W, Kistler WM. Spiking Neuron Models: Single Neurons, Populations, Plasticity. Cambridge, United Kingdom: Cambridge University Press; 2002

[35] Zhao C et al. Spike-time-dependent encoding for neuromorphic processors. ACM Journal on Emerging Technologies in Computing Systems (JETC). 2015;**12**(3):23

[36] Panzeri S et al. Sensory neural codes using multiplexed temporal scales. Trends in Neurosciences. 2010;**33**(3):111-120

[37] Boumans T et al. Neural representation of spectral and temporal features of song in the auditory forebrain of zebra finches as revealed by functional MRI. European Journal of Neuroscience. 2007;**26**(9):2613-2626

[38] Reich DS et al. Interspike intervals, receptive fields, and

information encoding in primary visual cortex. Journal of Neuroscience. 2000;**20**(5):1964-1974

[39] Brasselet R et al. Neurons with stereotyped and rapid responses provide a reference frame for relative temporal coding in primate auditory cortex. Journal of Neuroscience. 2012;**32**(9):2998-3008

[40] Shao L et al. Spatio-temporal Laplacian pyramid coding for action recognition. IEEE Transactions on Cybernetics. 2014;**44**(6):817-827

[41] Zhao C et al. Energy efficient spiking temporal encoder design for neuromorphic computing systems. IEEE Transactions on Multi-Scale Computing Systems. 2016;**2**(4):265-276

[42] Zhao C, Li J, Yi Y. Making neural encoding robust and energy efficient: An advanced analog temporal encoder for brain-inspired computing systems. In: Proceedings of the 35th International Conference on Computer-Aided Design. Austin, TX, USA: ACM; 2016

[43] Bai K, Yi Y. A path to energy-efficient spiking delayed feedback reservoir computing system for brain-inspired neuromorphic processors. In: Proceedings of 19th International Symposium in Quality Electronic Design (ISQED). 2018

[44] Bai K, et al. Enabling an new era of brain-inspired computing: Energy-efficient spiking neural network with ring topology. In: 2018 55th ACM/ESDA/IEEE Design Automation Conference (DAC). San Francisco, CA, USA: IEEE; 2018

[45] Ehsan MA, et al. Design challenges and methodologies in 3D integration for neuromorphic computing systems. In: 2016 17th international symposium on Quality electronic design (ISQED). Santa Clara, CA, USA: IEEE; 2016

[46] An H, Zhou Z, Yi Y. Opportunities and challenges on nanoscale 3D neuromorphic computing system. In: 2017 IEEE International Symposium on Electromagnetic Compatibility & Signal/Power Integrity (EMCSI). Washington, DC, USA: IEEE; 2017

[47] An H, et al. Electrical modeling and analysis of 3D neuromorphic IC with monolithic inter-tier vias. In: 2016 IEEE 25th Conference on Electrical Performance of Electronic Packaging And Systems (EPEPS). San Diego, CA, USA: IEEE; 2016

[48] An H, et al. Electrical modeling and analysis of 3D synaptic array using vertical RRAM structure. In: 2017 18th International Symposium on Quality Electronic Design (ISQED). Santa Clara, CA, USA: IEEE; 2017

[49] Yi Y, Zhou Y. Differential through-silicon-vias modeling and design optimization to benefit 3D IC performance. In: 2013 IEEE 22nd Conference on Electrical Performance of Electronic Packaging and Systems (EPEPS). San Jose, CA, USA: IEEE; 2013

[50] Ehsan MA, Zhou Z, Yi Y. Hybrid three-dimensional integrated circuits: A viable solution for high efficiency Neuromorphic Computing. In: 2017 International Symposium on VLSI Design, Automation and Test (VLSI-DAT). Hsinchu, Taiwan: IEEE; 2017

[51] Ehsan MA et al. A novel approach for using TSVs as membrane capacitance in neuromorphic 3-D IC. IEEE Transactions on Computer-Aided Design of Integrated Circuits and Systems. 2018;**37**(8):1640-1653

[52] An H et al. Monolithic 3D neuromorphic computing system with hybrid CMOS and memristor-based synapses and neurons. Integration, the VLSI Journal. 2017:1-9. https://reader.elsevier.com/reader/sd/pii/S0167926017

303413?token=CEB3CFF7957972E96D2
8980DF318ADC0F8B4F025E8A9116BF9
E7CDA0B67D8C5F61CC84371F37CC1D5
4A5510D6206547F

[53] An H et al. Three dimensional
memristor-based neuromorphic
computing system and its application
to cloud robotics. Computers and
Electrical Engineering. 2017;**63**:99-113

[54] Wong H-SP et al. Metal–oxide
RRAM. Proceedings of the IEEE.
2012;**100**(6):1951-1970

[55] An H, Zhou Z, Yi Y. Memristor-
based 3D neuromorphic computing
system and its application to associative
memory learning. In: 2017 IEEE
17th International Conference on
Nanotechnology (IEEE-NANO).
Pittsburgh, PA, USA: IEEE; 2017

[56] Clermidy F et al. Advanced
technologies for brain-inspired
computing. In: 2014 19th Asia and South
Pacific Design Automation Conference
(ASP-DAC). Suntec, Singapore: IEEE;
2014

[57] Swaminathan M. Electrical design
and modeling challenges for 3D system
integration. In: 12th International
Design Conference, Dubrovnik, Croatia.
2012

[58] Gourier N, Hall D, Crowley JL.
Estimating face orientation from robust
detection of salient facial structures.
In: FG Net Workshop on Visual
Observation of Deictic Gestures. 2004

Section 2

Bioactive Devices for Medical Applications

Nature-Inspired Processes and Structures: New Paradigms to Develop Highly Bioactive Devices for Hard Tissue Regeneration

Lorenzo Preti, Barbara Lambiase, Elisabetta Campodoni, Monica Sandri, Andrea Ruffini, Nicola Pugno, Anna Tampieri and Simone Sprio

Abstract

Material scientists are increasingly looking to natural structures as inspiration for new-generation functional devices. Particularly in the medical field, the need to regenerate tissue defects claims, since decades, biomaterials with the ability to instruct cells toward formation and organization of new tissue. It is today increasingly accepted that biomimetics is a leading concept for biomaterials development. In fact, there is increasing evidence that the use of biomedical devices showing substantial mimicry of the composition and multi-scale structure of target native tissues have enhanced regenerative ability. As a relevant example, biomimetic materials have high potential to solve degenerative diseases affecting the musculoskeletal system, namely, bone, cartilage and articular tissues, which is of pivotal importance for most of human abilities, such as walking, running, manipulating, and chewing. In this respect, the adoption of nature-inspired processes and structures is an emerging fabrication concept, uniquely able to provide biomaterials with superior biological performance. The chapter will give an overview of the most recent results obtained in the field of hard tissue regeneration by using 3D biomaterials obtained by nature-inspired approaches. The main focus is given to porous hydroxyapatite-based ceramic or hybrid scaffolds for regeneration of bone and osteochondral tissues in neurosurgery and orthopedics.

Keywords: biomineralization, biomorphic transformation, biomimetic hydroxyapatite, bioactive porous scaffolds, bone regeneration, osteochondral regeneration

1. Introduction: The biomimetic concept in biomaterials science

Biomimicry in biomaterials science means examining nature, its models, systems, processes, and elements to emulate or take inspiration from in order to solve human problems. The scientific community has now realized that in spite of recent advances, many societal needs are still unmet. Biologically inspired approaches have been particularly attractive in several fields, in over 3.8 billion years of evolution.

Several solutions were introduced with increased functionality reducing energy and materials and with no impact on environment, exactly the targets faced by the actual technological challenges [1, 2]. Biomimicry has engaged several fields creating smart materials to solve those problems that nature has already solved. In that past 50 years, some examples of biologically inspired materials were developed. In particular, exploiting bioinspired technologies bone-like materials based on wood and tough ceramics based on mother-of-pearl were designed. Despite biomedical field, other kinds of materials were created such as self-cleaning structures based on flowers, underwater glues based on mussel adhesive, drag reduction based on dermal riblet on shark skin, flight mechanisms based on insect flight, etc. [3–6]. The most recent researches increasingly take inspiration from the nature trying to mimic complex behavior typical of natural structures; in particular, new synthesis methods enabling controlled crystal growth and organized structures at the multi-scale levels are paying close attention. In this way nature is studied not only to develop biomimetic material but also to mimic natural process to create new materials. A highly mimicked natural process is biomineralization useful to create biocompatible materials very close to natural tissue. Biomineralization is a natural process by which organisms form minerals and consists in a complex cascade of phenomena generating hybrid nanostructured materials hierarchically organized from the nanoscale to the macroscopic scale. This process is at the basis of load-bearing structures such as bones, shells, and exoskeletons and allows designing biocomposite with unique properties, not obtainable with any conventional approach, as the information's exchange with cells and the trigger of the bone regenerative cascade [7, 8].

2. Biomimetic nano-apatites

In biology, calcium phosphates are the major inorganic constituents of bones, teeth, fish enameloid, deer antlers, and some species of shells [9]. Human hard tissues are composed principally of calcium phosphates with the exception of small portions of the inner ear. They are poorly crystalline carbonate-substituted nano-sized apatites, with the exception of enamel, which has a high degree of crystallinity. Nanocrystalline apatites are nonstoichiometric (Ca/P ratio less than 1.67) and calcium (and OH)-deficient and may incorporate substituted ions in the crystal lattice (Na^+, Mg^{2+}, K^+, Sr^{2+}, Zn^{2+}, etc.), in contrast to HA [$Ca_{10}(PO_4)_6(OH)_2$], which is the stoichiometric hydroxyapatite phase that is the most stable and least soluble calcium phosphate at physiological conditions. The nanocrystalline apatites exhibited higher solubility compared with HA; the responsible are calcium and hydroxide deficiencies. If they are submitted to humid environment, they are able to mature; as a result, "mature" bone crystals in vertebrates are less soluble and reactive than embryonic (young) bone mineral crystals [10].

The chemical composition of nanocrystalline apatites differs significantly from that of HA. The global chemical composition of biological apatites (or their synthetic analogues) can generally be described as

$$Ca_{10-x}(PO_4)_{6-x}(HPO_4 \text{ or } CO_3)_x (OH \text{ or } \tfrac{1}{2}CO_3)_{2-x} \text{ with } 0 \leq x \leq 2 \qquad (1)$$
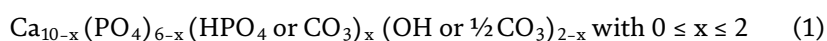
Minor substitutions are also found in biological apatites that involve monovalent cations (especially Na^+ and K^+), for example. In this case, charge compensation mechanisms must be taken into account.

The nanocrystalline apatites (whether biological or their synthetic analogues prepared under close-to-physiological conditions) could be probably described as the composition of an apatitic core (often nonstoichiometric) and a hydrated

surface layer containing water molecules and relatively weakly bound ions (e.g., Ca^{2+}, HPO_4^{2-}, CO_3^{2-}, etc.) [11] occupying non-apatitic crystallographic sites.

The hydrated surface layer is responsible for most of the properties of biomimetic apatites. The role of bone mineral in homeostasis in vivo could be explained by the high surface reactivity of biomimetic apatites in relation to surrounding fluids (which is probably directly linked to a high mobility of ionic species contained within this layer). The ions inside the hydrated surface can potentially be exchanged by other ions from the surrounding solution or by small molecules, which may be exploited for couplings with proteins or drugs. It is interesting to remark that during the aging of the nanocrystals, the typical non-apatitic features mentioned above tend to be progressive. This process that has been related to the progressive growth of apatite domains at the expense of the surface hydrated layer is called "maturation" [12].

The metastability of such poorly crystallized nonstoichiometric apatites, which steadily evolve in solution toward stoichiometry and better crystallinity, is thought to be linked to the maturation process. This evolution can be, for example, witnessed by the decrease of the amount of non-apatitic HPO_4^{2-} ions upon aging or else by the decreased potentialities to undergo ion exchanges [12].

Synthetic HA exhibits excellent biological properties such as biocompatibility, bioactivity, lack of toxicity, absence of inflammatory and immune responses, and relatively high bioresorbability. Improving their biomimetism, that is, by preparing them with dimensions, morphology, and nanostructure, can significantly enhance these properties and chemical characteristics that are similar to those found in biological apatites [9]. In the recent years, many different strategies have been employed in the preparation of synthetic nanosized HA crystals, with the most common method being stoichiometric titration of calcium hydroxide slurry with phosphoric acid up to neutrality.

Several methods have been successfully employed in the synthesis of nanocrystalline apatites, including wet chemical precipitation, sol-gel synthesis, coprecipitation, electrodeposition, vapor diffusion, and a number of others [13]. The physicochemical characterizations carried out on several synthesized apatites at low temperatures have shown that they have the typical features of biological apatite, such as the size domain, the low degree of crystallinity, and the existence of surface compositions different from the bulk [14, 15].

The method of ionic substitution has been proposed for improving not only the biomimetic features of apatite but also the biological performance of apatite-based materials. Many attempts have been made to synthesize HA that contains carbonate as a raw material for the manufacture of biomaterials. Carbonate can substitute for OH (A-type substitution) or for PO_4^{3-} (B-type substitution). A and B carbonated apatites can be distinguished by the different positions of the carbonate infrared absorption bands and by their different lattice constants. In biological apatites, CO_3^{2-} substitutes mainly for PO_4^{3-} in B-type apatite. Charge compensation by a Ca^{2+} vacancy, together with an H atom that bonds to a neighboring PO_4^{3-}, has been established to be the most stable arrangement. The incorporation of carbonate usually results in poorly crystalline structures with increased solubility, because it inhibits apatite crystal growth [16].

Divalent ions, such as magnesium and strontium, that replace calcium are particularly active during the first stages of the remodeling and regenerative processes. In particular, magnesium enhances skeletal metabolism and bone growth, so is associated with the first stages of new bone formation. Like carbonate, magnesium decreases with the aging of the bone and with increasing calcification. In synthetic HA, the presence of magnesium increases the chemical-physical mimesis of the mineral bone. In fact, magnesium affects the kinetics of HA nucleation on collagen,

increasing it, and retards its crystallization, affecting the shape and size of mineral nuclei. The substitution of Ca^{2+} with Mg^{2+} into the HA structure leads to a continuous ion exchange from the outer hydrated layer to the well-crystallized apatite lattice, inducing a disordered state on the HA surface. Moreover, the incorporation of magnesium in surface crystal sites increases the number of molecular layers of coordinated water; all of these phenomena favor the adhesion of cells to the scaffold because the protein adsorption is increased. A greater osteoconductivity over time and higher material resorption, compared to stoichiometric HA, were detected in granulated Mg-HA powders that were implanted in a rabbit's femur, proving the increase of osteogenic activity in the presence of magnesium-substituted HA. A higher expression of specific markers of osteoblast differentiation and bone formation, which are associated with a lower osteoclastogenic potential, was revealed by studies of osteoblast gene expression profiles from Mg-HA grafts [17, 18].

The incorporation of strontium into the HA structure reduces bone resorption while enhancing osteogenesis; this effect improves physical stabilization of the new bone matrix, enhancing collagen synthesis, as shown in in vitro and in vivo studies. The incorporation of strontium ions into the HA lattice has been practiced in recent years, due to its potential as an anti-osteoporotic agent, and increasing effort is being dedicated to the development of strontium-containing bone cements [19].

Biomimetic HA powders can be synthesized and used as granules to fill bone defects of limited size, but if the regeneration of an extended bone part is necessary, the implantation of a 3D porous scaffold is required because the lack of mechanical stability and specific morphology of granulated bio-devices does not enable regeneration of extended bone segments; therefore, the porous scaffold must have, in addition to bioactivity and osteoconductivity characteristics, also biomechanical performance suitable for the specific implant site. The scaffolds must provide both the space for the new bone formation and the necessary support for the cells to proliferate and maintain their differential function. Furthermore, they should present suitable architectures for inducing the formation and maturation of well-organized tissue. The use of bioactive scaffolds aids the process of osteoconductivity that establish physical and mechanical integration with the surrounding bone, which in turn avoids micro-movements and the possibility of early mechanical loading in vivo [20].

3. Porous hydroxyapatite scaffolds for bone regeneration

Bone scaffolds are intended as 3D porous bodies that can allow efficient cell colonization and neovascularization of newly formed tissues throughout the whole implant [21], also giving tight mechanical attachment to the porous scaffold. This is a key achievement for the stabilization of the defect and the recovery of bone-like mechanical performance [22, 23].

Different technologies have been investigated for the development of bone scaffolds with bone-like porosity associated to adequate biomechanical strength [24]. All techniques are based on sintering processes for the consolidation of porous structures formed by processing of ceramic suspensions. Many of them make use of sacrificial phases that are later removed by controlled processes. Methods using sacrificial templates use porogenic agents, such as polymer components, mainly, but also natural sources and inorganic-soluble salts, dispersed into ceramic suspensions and then decomposed by thermal treatments or extracted by chemical processes. The replica method uses organic sacrificial templates but, in the form of 3D bodies, is also derived by natural sources such as cellulose sponges [25], which are eliminated by burning after being soaked into ceramic suspensions.

Other very efficient techniques use the formation of bubbles driven by chemical components dispersed in the suspensions or the direct introduction of gases in the ceramic slurries to obtain foamed powder suspensions, which are sintered after casting and drying [26]. The key aspect in such direct foaming methods is to accurately control the suspension rheology by the use of stabilizing agents (**Figure 1**).

Due to controlled macroporosity and pore interconnection obtained by this flexible method, scaffolds not only exhibit improved osteoconductive ability but also higher mechanical properties than those obtained using sacrificial templates [24]. A recent study reported a novel promising route based on a modified direct foaming method that gave HA bodies with 65% pore volume and a compressive strength $\sigma = 16.3 \pm 4.3$ MPa [27].

A relevant field of application for porous bone scaffolds is neurosurgery; here, cranial reconstruction often uses synthetic biomaterials implants (polymers, metals, and ceramics) instead of autologous bone [28], particularly for large bone defects. An important issue in this respect is the occurrence of bone resorption and infection, which can result in the removal of the implant and its replacement with other materials [29]. Nowadays, polymethyl methacrylate (PMMA) is the first option among synthetic materials for cranioplasty mainly because of its excellent tensile strength [30]; but its potential decomposition into the starting monomer may lead to fracture susceptibility, other than inflammation and infection [31]. To strengthen the prosthesis, titanium wire mesh is often used as a support for the acrylate thanks to its overall high strength and malleability [32]. Also, polyetheretherketone (PEEK), possessing mechanical strength and elasticity similar to natural bone, is involved as implant for cranial reconstruction [33].

However, all these synthetic materials have the limitation of being bioinert: they have poor osteogenic and osteoconductive ability, so their implants may not integrate tightly with the surrounding newly formed bone [28].

An interesting alternative is in the use of synthetic porous HA ceramic that, due to its good bioactivity deriving from biomimetic composition, can stimulate new bone formation and tight integration of bone to the prosthesis, with recovery of the original biomechanical performance [34, 35].
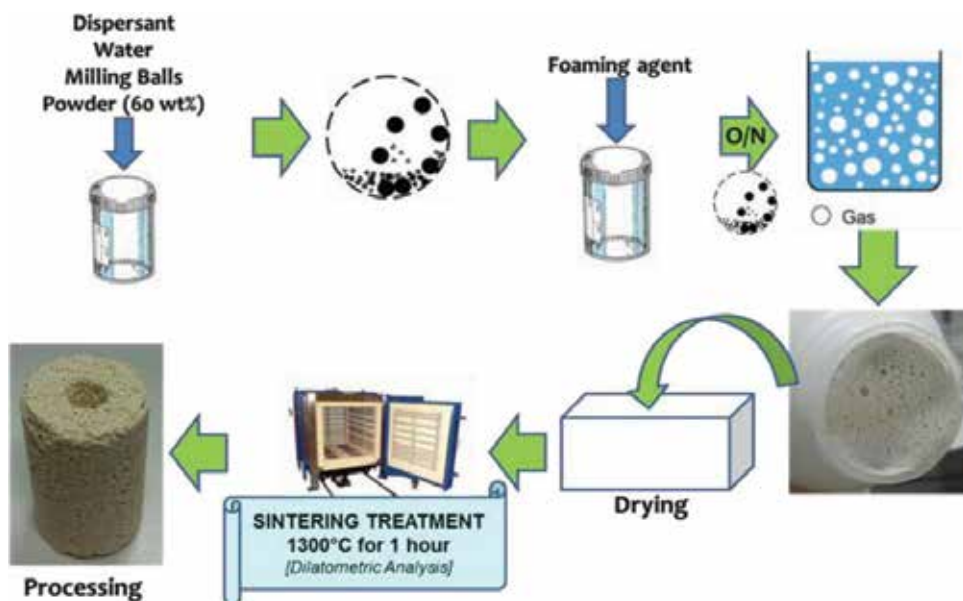
Figure 1.
Scheme of the direct foaming process to obtain 3D bioceramic porous scaffold.

Despite the advantages, HA is reported to have the tendency to fragmentation due to its brittle character, typical of ceramic materials [28], which do not allow its use for load-bearing bone (e.g., femur, tibia, and metatarsus) reconstruction. In this respect, the current research in scaffold materials is directed toward the design and development of bioactive ceramic composites, especially as biodegradable implants, with bone-like three-dimensional structure and improved mechanical performances. Several attempts were made to join a bioactive/bioresorbable component (particularly HA and other calcium phosphates, such as tricalcium phosphate (TCP)) and a bioinert/bioactive reinforcing phase (ZrO_2, calcium silicates, Al_2O_3, TiO_2, and others) [36–38]. Among them TCP/TiO_2 composites are considered very interesting for bone regeneration because β-TCP presents accelerated degradation and optimal reactivity with the bone tissue, thanks to its calcium to phosphorus ratio lower than that of HA [38], while TiO_2 can form a tightly bound superficial HA layer, thanks to its bioactivity, and presents high mechanical performances [39, 40].

It has been recently demonstrated that dense and porous TCP/TiO_2 bodies, obtained by optimized sintering process, display high values of flexural strength and fracture toughness, thanks to the presence of a reinforcing network made of TiO_2-coalesced nanoparticles [41]. Moreover, increased proliferation, colonization, and viability were found demonstrating good osteogenic properties, thus showing good potential as scaffolds for load-bearing bone reconstruction [42].

4. Injectable self-hardening bone cements with biomimetic composition and nanostructure

Bone diseases, such as hemangioma, multiple myeloma, osteolytic metastases, and osteoporosis, can yield bone weakening, thus commonly resulting in fractures in the vertebrae, femur, and radius, especially in the elderly [43]. Minimally invasive surgery procedures, such as vertebroplasty and kyphoplasty, are currently used to regenerate osteoporotic fractures with bone cements as bone defect fillers [44].

Ideally, bone cements should exhibit adequate mechanical support to withstand the early biomechanical loads and should establish effective integration with newly formed bone. The most common injectable cements are based on polymethyl methacrylate (PMMA), thanks to their favorable mechanical properties and robustness [45]. However, PMMA bone cements lack the necessary bioactivity and resorbability, for which it is a foreign body presenting excessive rigidity, in comparison with the bone, so to potentially provoke secondary fractures at adjacent vertebrae. Moreover, PMMA hardening occurs through an exothermic polymerization process, leading to the risk of thermal necrosis of the surrounding bone tissue [46]. In contrast with these drawbacks, calcium phosphate-based bone cements (CPCs) have attracted great attention due to their excellent bioactivity, deriving from the chemical similarity with the bone tissue, and bioresorbability, which lead to the formation of new bone that can replace the implant [47, 48].

Numerous CPC formulations with different initial reactants (which include α-tricalcium phosphate, β-tricalcium phosphate, anhydrous dicalcium phosphate, and monocalcium phosphate monohydrate), producing either an apatitebased or brushite-based cement [49], have been reported [50, 51]. In addition to their excellent biological behavior, CPCs are intrinsically microporous: pores in the size range of submicro-/micrometers are left by extra aqueous solution after hardening of CPCs [52]; such micropores are effective for the impregnation of biological fluids into the bone cements and help resorption and replacement of implants by bone.

One of the most critical issues of injectable CPCs is the control of the chemistry of setting reactions and rheological properties, to achieve adequate injectability, setting time, and mechanical properties [53]. A recent interesting approach involves the addition of natural polymers or their derivatives, such as sodium alginate [54], hydroxypropyl methylcellulose [55], hyaluronic acid [56], chitosan [57], and modified starch [58], into the starting powder or in solution into the cement paste [59]. Biopolymers can be developed as low-viscosity solutions for easy injection and have the ability to cross-link in situ after injection under physiological conditions (temperature or pH) or by the action of an initiator (light or cationic cross-linkers) [53]. In general, due to the higher viscosity of the CPC paste, the presence of polymers tends to increase setting time and to enhance CPC injectability and cohesion. Furthermore, the use of biopolymeric additives can be an effective method to improve the mechanical performance of CPCs [53]. Depending on the final CPC properties desired, different polymers may be incorporated into CPCs, and the polymeric solution may be altered by changing concentration, molecular weight, and polymer chain length [59].

Among the several approaches proposed for the synthesis of CPCs, the use of α-tricalcium phosphate (α-TCP) powder [60] as a metastable precursor is particularly of interest for introduction of foreign ions, such as Mg^{2+}, CO_3^{2-}, SiO_4^{4-}, and Sr^{2+}, enhancing bioactivity and providing efficient therapies against degenerative bone diseases [19, 20, 61].

In particular, CPC formulations based on Sr-doped apatitic cements are very interesting because of strontium ability to enhance cell proliferation and differentiation into bone-forming osteoblasts and decrease the resorbing activity of mature osteoclasts; this is a key achievement for the restoration of the bone turnover balance, especially when the cement is used to treat osteoporotic bone fractures [62]. Sr-substituted TCP was shown to slow down the cement setting as well as the transformation into Sr-doped HA. Moreover, due to apatite lattice expansion, the introduction of strontium in the apatite structure is associated with an increased solubility of the cements, leading to an increase of ions released, which in turn was found to have a positive effect on cell proliferation and osteogenic differentiation [62]. In particular, Sr-substituted CPCs previously tested in vivo exhibited increased new bone formation compared to Sr-free CPCs. Due to the different preparation routes and properties of the set samples, such as phase composition and porosity, contradicting results of Sr effect on the mechanical characteristics of substituted CPCs can be found. In most compositions setting into Sr-HA, strontium substitution either increased compressive strength or had no significant effect on the mechanical characteristics [63].

Recently, novel injectable, self-setting Sr-HA bone cements were prepared by mixing Sr-substituted α-TCP phases as unique inorganic precursors with disodium phosphate solutions enriched with alginate. In vitro tests showed that different concentrations of Sr^{2+} were able to promote an inductive effect on mesenchymal stem cell differentiation, especially at 2 mol% concentration, and on pre-osteoblast proliferation and an inhibitory effect on osteoclasts activity [64]. Moreover, the addition of alginate significantly improved both injectability and cohesion, leading also to significantly higher compression strength when compared with alginate-free cements, without affecting the hardening process and with the absence of cytotoxic effects. On the basis of these results, a selected Sr-HA cement formulation was further tested in vivo in a rabbit model by compositional, morphological, and histological/histomorphometric analysis. The cement exhibited complete transformation into HA, thus showing a biomimetic composition, and enhanced the ability to induce new bone formation and penetration, provided also by its porous microstructure [65].
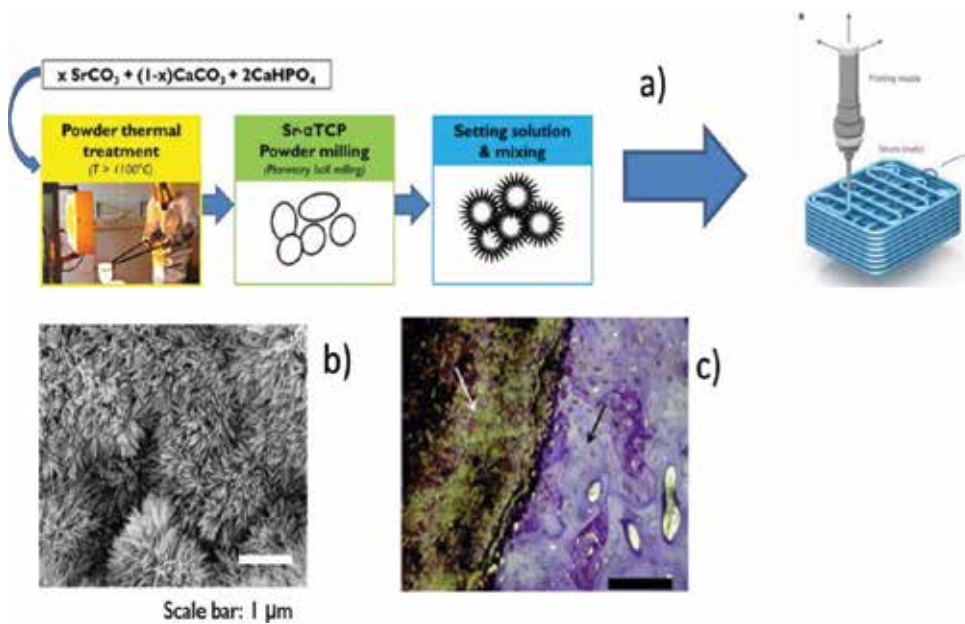
Figure 2.
(a) Scheme of the development of self-hardening formulations as printable pastes, (b) typical nanostructure of hardened apatite cements, and (c) very tight interface between Sr-substituted apatite cement and bone in rabbit test.

Ion-doped apatites obtained as bone cements offer interesting perspectives as a new class of injectable biomaterials that can found application as bioactive pastes for the regeneration of bone defects with complex geometry and not easily accessible by implantation of 3D solid scaffolds (e.g., femur head, tibial plateau, vertebral body, and maxilla). A very interesting perspective, further extending the possible application of bioactive pastes and cements, is the development of printable self-hardening biomaterials (**Figure 2**). Such pastes, to be prepared with rheologic properties enabling flowability, cohesion, and hardening in short times, to allow layer-by-layer deposition, can be processed by micro-extrusion to obtain solid scaffolds with enhanced bioactivity, thanks to the possibility to maintain biomimetic chemical composition, without the need of conclusive sintering process for consolidation.

5. Hybrid scaffolds obtained by bioinspired assembling/mineralization process for bone and osteochondral regeneration

Hard tissues are biological constructs incorporating minerals into soft matrix to create a protective shield or a structural support such as the bone, teeth, and cartilage [7]. The non-mineralized region, called also soft tissue, can be connective, muscular, nervous, or epithelial. Especially examining bone tissue, it is a highly dynamic and vascularized tissue which has an ability to self-heal and remodel through a well-orchestrated process; the bone remodeling is a constant process, targeting to replace odd bone through resorption by means of osteoclasts and to produce new bone by means of osteoblast which usually completes in 4–6 months. However, the high regenerative capacity is lost when there is a large segmental defect, severe non-unions, or bone tumor resection [66]. To overcome these issues, the concept of bone tissue engineering (BTE) has been developed producing

tailor-made scaffolds with the ability to fine-tune the tissue regeneration process. Four different biological prerequisites are necessary for BTE such as osteogenic cells, osteoinductive stimulus, osteoconductive matrix scaffolds, and mechanical environment which led to design scaffolds with appropriate macroporous structure, good degradability, and better osteoconductive properties [67]. A 3D structure is not enough to obtain a material with osteoinductive stimulus, but the chemical composition plays a decisive role. Both concepts (chemical composition and 3D architecture) are at the basis of biomimicry; hence, to obtain scaffolds with chemical composition very close to natural bone, a bioinspired synthesis method mimicking the natural biomineralization process was carried out [68].

In this respect, previous studies by Tampieri et al. exploiting the biomineralization process abovementioned developed biocomposites made of collagen and hydroxyapatite for bone and osteochondral regeneration [69–71].

Exactly as it happens in nature, collagen molecules promoted complex 3D arrangement and the heterogeneous nucleation of a low crystalline hydroxyapatite also due to the incorporation of foreign ions, usually present in human tissue, into the apatite phase. In details, biomineralization process was reproduced in the laboratory dropping an acid solution containing PO_4^{3-} ions mixed with collagen gel into an alkaline solution containing the Ca^{2+} ions exploiting a neutralization process. The pH of the suspension is increased up to neutral pH where two different mechanisms are simultaneously triggered; on the one hand, the collagen fibers reach the isoelectric point leading to their assembly into a 3D network; on the other hand, the mineral nucleation starts in correspondence to the carboxylic groups exposed by the collagen molecule that bind calcium ions [69–72]. One of the advantages of this material is the capability to entrap some foreign ions into HA lattice obtaining a hybrid material mimicking natural mineralized tissues. In particular, CO_3^{2-} ions can occupy two different sites of the apatite lattice. B-substitution occurs at the PO_4^{3-} site improving the osteoblasts adhesion and is typical of young and immature bones; conversely, carbonation in site A refers to partial substitution of OH^-, which increases the stability of mineral phase, and in fact it is more typical of mature bone tissue. Mg^{2+} promotes the HA nucleation and bioavailability decreasing the crystallinity. Sr^{2+} is able to restore the bone turnover balance; this is important for the treatment of osteoporotic bone fractures [73, 74].

The aptitude of the apatite lattice to host several isovalent and heterovalent ion substitutions permits to synthesize apatite nanocrystals with multiple substitutions that can be used in different applications in regenerative medicine and nanomedicine. Furthermore, besides the incorporation of foreign ions, also the control mechanisms exerted by the organic phase allow to produce a more biomimetic apatite thanks to nearly amorphous crystal state and crystal orientation; in this way, cells well recognize hybrid composite without any inflammatory reaction and start to interact with it promoting the adhesion and proliferation on its fibers [75, 76]. Therefore, the use of bioinspired mineralization process is a tool able to confer unique properties to hydroxyapatite otherwise impossible to find in stoichiometric hydroxyapatite as well as in composites where hydroxyapatite was simply mixed with collagen [70].

Among bone defects, large chondral articular defects represent a major problem in orthopedic practice [77], and tissue engineering is providing promising results [78]. However, the results for the treatment of cartilage lesions are still controversial, and osteochondral lesions are even more severe relating to two different tissues featuring different self-healing abilities and cell lineages involved. 3D scaffold, usually, is able to well regenerate a single tissue, as cartilage tissue, and in case of osteochondral damage, additional autologous bone grafting is often necessary [79]. To overcome these limitations and to increase the advantages for osteochondral

regeneration, biomaterials provide the template for tissue development that can be adjusted in shape, size, and orientation according to defect features [80].

For this reason, several authors have highlighted the need to modulate a multi-layered scaffold capable to reproduce different biological and functional environments of osteochondral region to promote regeneration [80, 81]. To create construct with more favorable integrative properties in the osteochondral site, bilayer or tri-layer composite is developed such as a polylactide-co-glycolide copolymer, the first scaffold reported for clinical use; however, it showed poor repair tissue quality at imaging, as well as unsatisfactory clinical outcomes [82, 83]. One of the difficult points in the osteochondral regeneration is the interface between material's layer and host tissue and between layers of host tissue; the cartilage repair should be followed by an adequate regeneration of the subchondral structure and by the effective union with surrounding host tissue [84]. Tampieri et al. designed a composite scaffold consisting of three different but integrated layers, corresponding to cartilage, calcified cartilage, and bone components [69]. It was developed to better mimic structure and composition of the whole osteochondral unit, showing promising clinical results even in challenging conditions, such as complex lesions or osteoarthritic knees [85, 86]. Exploiting biomineralization process, a different extent of mineralization was nucleated on collagen fibers developing a tri-layer with a gradient of hydroxyapatite ranging from a mineral content of 60–70% corresponding to subchondral bone and 30–40% corresponding to mineralized cartilage up to 0% corresponding to hyaline cartilage (**Figure 3**). Furthermore, in the top layer (hyaline cartilage), hyaluronic acid was added to create microstructural features improving the hydrophilic ability to reproduce columnar-like structure converging toward the external surface, where it formed horizontal flat ribbons, thus resembling the morphology of the *lamina splendens*.

Chemical-physical investigation highlighted that chemotactic information provided by collagen-induced unique features in the inorganic phase, promoting the nucleation of a biomimetic apatite very close to the biological one present in the bone [87]. In vivo evaluation demonstrates that it differentially supports cartilage and bone tissue formation in the different histological layers [88]. After 6 months from implantation of graded hybrid composites on femoral condyles of
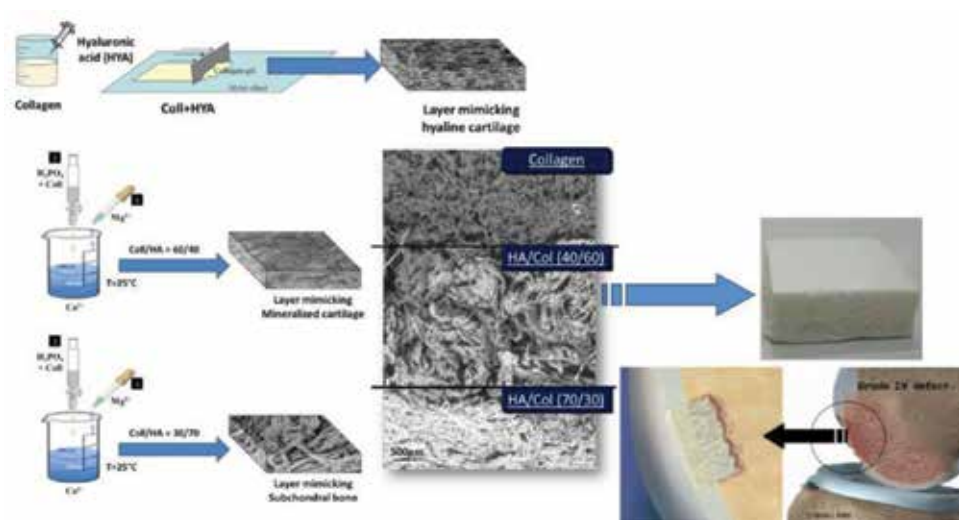
Figure 3.
Representation of multilayered hybrid scaffold obtained by in-lab biomineralization and its application in osteochondral defect.

sheep, a new hyaline-like tissue is formed, and a good integration of scaffolds with host cartilage is observed; furthermore, a strong proteoglycan staining, columnar rearrangement of chondrocytes, and an underlying well-structured subchondral trabecular bone are shown. Besides, hybrid scaffold was completely resorbed, and no remarkable difference was revealed with or without seeding of chondrocyte cells, highlighting as chemical-physical features of hybrid composite allow the recruitment of bone marrow stem cells directly from the underlying subchondral bone [88].

In conclusion, the ability of the scaffold to induce orderly osteochondral tissue repair without the introduction of cells makes it attractive for several reasons: (i) from a practical and commercial standpoint, because it could be used as an off-the-shelf graft in a one-step surgical procedure; (ii) from a surgical standpoint, it could be inserted under minimally invasive conditions due to its flexibility; and (iii) from a biological standpoint, because the problems related to the cell culture would be eliminated [89].

6. Biomorphic transformation of natural structures: a new way to obtain biomimetic scaffolds for regeneration of load-bearing segmental bones

Among the bone diseases, those affecting portions of long bone subjected to mechanical loads are the ones which most seriously impact on the quality of life of sufferers. The incidence of such pathologies is particularly relevant among the aged people (osteoporosis); anyway, more recently the number of relatively young patients affected by bone diseases has increased mainly owing to modern lifestyles (e.g., intense sport activity, obesity, etc.). In this case, pain and disability also impact on the psychological well-being, leading to anxiety, depression, fear for the future, and altered perception of the social role. Such feeling is nowadays shared by the aged people also, because of the increased expectation of an active life and well-being even among the elderly. For this reason, the abovementioned numbers in terms of socioeconomic costs and number of hospitalized people are likely to increase in the next future.

Due to the inability of the current manufacturing technologies to form mechanically strong porous inorganic structures with a hierarchic pore organization and complex morphological details in the submicron scale, the healing of load-bearing bone segments still relies on bioinert dense implants based on alumina, titanium, etc.

A significant change in engineering and ceramic processing is needed, thus greatly expanding the existing tools enabling the development of porous and massive ceramic bodies with designed smart functions. The current manufacturing approach in ceramic development is based on powder synthesis, forming, and thermal consolidation (sintering); the idea is to surpass the existing approach, by developing new "one-step synthesis/consolidation processes" to obtain new 3D ceramics with properties and functions not achievable with the current manufacturing approach. In particular, this is relevant when the ceramic phases with desired functional properties have low thermodynamic stability such as nanosized and atomic position, so that the existing ceramic process, particularly sintering, destroys labile phases increasing their stability but deleting its smart functional properties. Particularly, the sintering process, which is fundamental to consolidate ceramic bodies, impairs the maintenance of ceramic phases characterized by low crystallinity, nanosize, and nonstoichiometric composition. These features, relying on low thermodynamic stability, are very often the source of functions that cannot be expressed by a stable, sintered ceramic phase [20].

The main goal is the implantation of osteoinducting and osteoconducting scaffolds with spatially organized macroporosity and mechanical strength sufficient for early in vivo loading upon implantation and elastic properties close to those of the bone. This may enable scaffolds to respond to the biomechanical loads and activate mechano-transduction mechanisms, yielding remodeling and formation of new functional bone [90]. The complex structure of bones, hierarchically organized from the nano- to the macro-scale, and the interaction taking place across all levels of organization are the reasons of the outstanding mechanical performances of bones. For this reason, long-bone regeneration should be assisted by scaffolds endowed with bone-like composition and similar structural complexity; however, the common manufacturing methods do not produce mechanically resistant scaffolds with the required hierarchical pore organization and bioactivity. The chemical biomimesis in scaffolds for long-bone regeneration is influenced by the mechanical strength of HA-based materials. There are several studies about scaffolds based on composite materials, making use of strong bioactive or bioinert phases [36, 37] that were dispersed in a calcium-phosphate matrix. However, the limitation in the achievement of hierarchically organized structures still remains [8].

This problem can reside in nature, so the attention of scientists has been moved to find and observing complex morphologies that exist in nature, and then try to reproduce them. In particular, the ligneous structures strongly resemble bones in their structural organization and morphology which affect the mechanical performances [8].

Like bone, wood can be considered as a cellular material at the scale of hundred micrometers to centimeters (**Figure 4**). At the cell level, the mechanical properties are governed by the shape and diameter of the cell cross section, as well as by the thickness of the cell wall. In particular, the apparent density of wood, which in turn is a determining factor for the performance of lightweight structures, is directly related to the ratio of cell wall thickness to cell diameter. The particular hierarchical architecture of the cellular microstructure gives wood an exceptional combination of high stiffness, toughness, and strength at low density [91]. The alternation of channel-like porous and fiber bundle areas makes the wood an elective material to be used as a template in the preparation of a new bone substitute that is characterized by a biomimetic hierarchical structure [20].
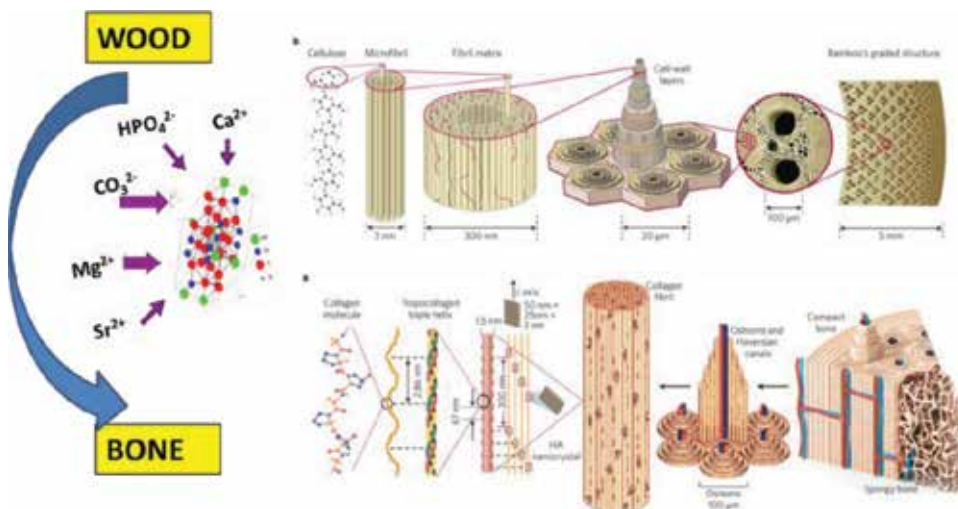

Figure 4.
Scheme of the multi-scale structure of wood and bone tissue.

A subject of investigation in the late 1990s was the transformation of wood into inorganic, hierarchically organized materials (e.g., oxidic ceramics such as Al_2O_3, ZrO_2, TiO_2, and MnO and nonoxidic ceramics such as SiC, TiC, and ZrC) [92–96]. The synthesis of hierarchically organized bone scaffolds made of SiC is a result of these studies [94], which have the advantage of offering bio-tolerated surfaces and very high fracture strength. Other kinds of biomorphic transformations, conceived recently, were used to manufacture hierarchically organized scaffolds made of HA [3]. The complexity of the apatite phase, in comparison with nitrides, carbides, and oxides, required the settling of a multistep process transformation, where the native wood was sequentially transformed into pure carbon, calcium carbide, calcium oxide, calcium carbonate, and finally HA. Due to their bone-mimicking hierarchical organization, microstructure and composition such a new generation of bioceramics scaffolds promise to offer enhanced integration, osteogenesis, and biomechanical behavior when implanted in vivo [8].

Woods such as rattan have strong similarities to 3D structure and morphology of cortical and spongy bone. Rattan is characterized by channel-like pores (simulating the Haversian system in bone), interconnected with a network of smaller channels (such as the Volkmann system) [3].

There is a precise control of the microstructure, crystallinity, and phase composition, during the multistep transformation process, in which different gas-solid reactions occur where the solid is the template. Calcium, oxygen, carbonate, and phosphate ions were progressively added in the different steps to finally get the HA molecules. The reaction kinetic is controlled throughout the different steps of the transformation process in order to have a precise control of the scaffold microstructure, composition, and bioactivity [95]. Importantly, even in the absence of thermal consolidation treatments, the scaffolds exhibit mechanical strengths comparable to those of spongy bone (~4 MPa) when measured along the channel direction, thanks to the maintenance of the original wood microstructure.

The establishment of biomorphic transformations that are able to transform woods into biomimetic bone scaffolds can provide solutions for long-bone regeneration and can be designed in a custom-made fashion. Selected wood structures could reproduce different bone portions that are characterized by different porosities and pore distributions, as occurring in cortical and spongy bones. Such devices may implement the formation of a biological chamber in vivo that contain a suitable environment that allows to promote and enhance bone formation and remodeling. The implant will thus function as an in vivo bioreactor, thus facing an unsolved clinical problem related to the disappearing of the regenerative process at distances far from the bone-implant interface [20].

7. Conclusions and future perspectives

The progressive population aging and the younger people modern behaviors, which expose to serious injuries and traumas, are concerns of large and continuously increasing socioeconomic impact. The continual advances in materials science and nanotechnology allowed great progress in biomedical device development for bone regeneration. Nevertheless, the development of bio-devices mimicking biological tissue structure and composition with high complexity and load-bearing properties, such as extended bone and osteochondral parts or segmental bones, still presents serious limitations. In fact, the related clinical needs remain unmet because of the absence of well-established regenerative devices for such applications. Many possibilities for solving these concerns are offered by the recent advances in materials science: the new-generation smart multifunctional device development could

be enabled by new fabrication approaches that get inspired from the multitude of outstanding biological structures and phenomena. The preliminary steps that have already been taken in this direction are very promising, and the development of bioinspired materials is rapidly becoming a priority to achieve nanotechnological solutions facing critical societal needs.

Conflict of interest

The authors declare no conflicts of interest.

Author details

Lorenzo Preti[1,2], Barbara Lambiase[1], Elisabetta Campodoni[1], Monica Sandri[1], Andrea Ruffini[1], Nicola Pugno[2], Anna Tampieri[1] and Simone Sprio[1]*

1 Institute of Science and Technology for Ceramics-National Research Council (ISTEC-CNR), Faenza, Italy

2 Laboratory of Bio-Inspired and Graphene Nanomechanics, Department of Civil, Environmental and Mechanical Engineering, University of Trento, Trento, Italy

*Address all correspondence to: simone.sprio@istec.cnr.it

IntechOpen

References

[1] Youngblood JP, Sottos NR. Bioinspired materials for self-cleaning and self-healing. MRS Bulletin. 2008;**33**(8):732-741. DOI: 10.1557/mrs2008.158

[2] Canejo JP, Borges JP, Godinho MH, Brogueira P, Teixeira PIC, Terentjev EM. Helical twisting of electrospun liquid crystalline cellulose micro- and nanofibers. Advanced Materials. 2008;**20**(24):4821-4825. DOI: 10.1002/adma.200801008

[3] Tampieri A, Sprio S, Ruffini A, Celotti G, Lesci IG, Roveri N. From wood to bone: Multi-step process to convert wood hierarchical structures into biomimetic scaffolds for bone tissue engineering. Journal of Materials Chemistry. 2009;**19**(28):4973-4980. DOI: 10.1039/B900333A

[4] Munch E, Launey ME, Alsem DH, Saiz E, Tomsia AP, Ritchie RO. Tough, bio-inspired hybrid materials. Science. 2008;**322**(5907):1516-1520. DOI: 10.1126/science.1164865

[5] Lee BP, Messersmith PB, Israelachvili JN, Waite JH. Mussel-inspired adhesives and coatings. Annual Review of Materials Research. 2011;**41**:99-132. DOI: 10.1146/annurev-matsci-062910-100429

[6] Pu X, Li G, Huang H. Preparation, anti-biofouling and drag-reduction properties of a biomimetic shark skin surface. Biology Open. 2016;**5**(4):389-396. DOI: 10.1242/bio.016899

[7] Weiner S. Biomineralization: A structural perspective. Journal of Structural Biology. 2008;**163**(3):229-234. DOI: 10.1016/j.jsb.2008.02.001

[8] Fratzl P, Weinkamer R. Nature's hierarchical materials. Progress in Materials Science. 2007;**52**(8):1263-1334. DOI: 10.1016/j.pmatsci.2007.06.001

[9] Roveri N, Palazzo B, Iafisco M. The role of biomimetism in developing nanostructured inorganic matrices for drug delivery. Expert Opinion on Drug Delivery. 2008;**5**(8):861-877. DOI: 10.1517/17425247.5.8.861

[10] Rey C, Combes C, Drouet C, Lebugle A, Sfihi H, Barroug A. Nanocrystalline apatites in biological systems: Characterisation, structure and properties. Materialwissenschaft und Werkstofftechnik. 2007;**38**(12):996-1002. DOI: 10.1002/mawe.200700229

[11] Drouet C, Bosc F, Banu M, Largeot C, Combes C, Dechambre G, et al. Nanocrystalline apatites: From powders to biomaterials. Powder Technology. 2009;**190**(1-2):118-122. DOI: 10.1016/j.powtec.2008.04.041

[12] Sakhno Y, Bertinetti L, Iafisco M, Tampieri A, Roveri N, Martra G. Surface hydration and cationic sites of nanohydroxyapatites with amorphous or crystalline surfaces: A comparative study. Journal of Physical Chemistry C. 2010;**114**(39):16640-16648. DOI: 10.1021/jp105971s

[13] Iafisco M, Morales JG, Hernández-Hernández MA, García-Ruiz JM, Roveri N. Biomimetic carbonate-hydroxyapatite nanocrystals prepared by vapor diffusion. Advanced Engineering Materials. 2010;**12**(7):B218-B223. DOI: 10.1002/adem.201080003

[14] Bertinetti L, Drouet C, Combes C, Rey C, Tampieri A, Coluccia S, et al. Surface characteristics of nanocrystalline apatites: Effect of Mg surface enrichment on morphology, surface hydration species, and cationic environments. Langmuir.

2009;**25**(10):5647-5654. DOI: 10.1021/la804230j

[15] Bertinetti L, Tampieri A, Landi E, Ducati C, Midgley PA, Coluccia S, et al. Surface structure, hydration, and cationic sites of nanohydroxyapatite: UHR-TEM, IR, and microgravimetric studies. Journal of Physical Chemistry C. 2007;**111**(10):4027-4035. DOI: 10.1021/jp066040s

[16] Boanini E, Gazzano M, Bigi A. Ionic substitutions in calcium phosphates synthesized at low temperature. Acta Biomaterialia. 2010;**6**(6):1882-1894. DOI: 10.1016/j.actbio.2009.12.041

[17] Bertinetti L, Tampieri A, Landi E, Martra G, Coluccia S. Punctual investigation of surface sites of HA and magnesium-HA. Journal of European Ceramic Society. 2006;**26**(6):987-991. DOI: 10.1016/j.jeurceramsoc.2004.12.037

[18] Landi E, Logroscino G, Proietti L, Tampieri A, Sandri M, Sprio S. Biomimetic Mg-substituted hydroxyapatite: From synthesis to in vivo behaviour. Journal of Materials Science: Materials in Medicine. 2008;**19**(1):239-247. DOI: 10.1007/s10856-006-0032-y

[19] Landi E, Tampieri A, Celotti G, Sprio S, Sandri M, Logroscino G. Sr-substituted hydroxyapatites for osteoporotic bone replacement. Acta Biomaterialia. 2007;**3**(6):961-969. DOI: 10.1016/j.actbio.2007.05.006

[20] Tampieri A, Iafisco M, Sprio S, Ruffini A, Panseri S, Montesi M, et al. Hydroxyapatite: From nanocrystals to hybrid nanocomposites for regenerative medicine. In: Antoniac IV, editor. Handbook of Bioceramics and Biocomposites. Switzerland: Springer International Publishing; 2015. pp. 1-26. DOI: 10.1007/978-3-319-09230-0_6-1

[21] Sprio S, Sandri M, Iafisco M, Panseri S, Filardo G, Kon M, et al. Composite biomedical foams for engineering bone tissue. In: Netti PA, editor. Biomedical Foams for Tissue Engineering Applications. Cambridge: Woodhead Publishing; 2014. pp. 249-280. DOI: 10.1533/9780857097033.2.249

[22] Babis GC, Soucacos PN. Bone scaffolds: The role of mechanical stability and instrumentation. Injury. 2005;**36**(4):S38-S44. DOI: 10.1016/j.injury.2005.10.009

[23] Woodard JR, Hilldore AJ, Lan SK, Park CJ, Morgan AW, Eurell JAC, et al. The mechanical properties and osteoconductivity of hydroxyapatite bone scaffolds with multi-scale porosity. Biomaterials. 2007;**28**(1):45-54. DOI: 10.1016/j.biomaterials.2006.08.021

[24] Studart AR, Gonzenbach UT, Tervoort E, Gauckler LJ. Processing routes to macroporous ceramics: A review. Journal of the American Ceramic Society. 2006;**89**(6):1771-1789. DOI: 10.1111/j.1551-2916.2006.01044.x

[25] Tampieri A, Celotti G, Sprio S, Delcogliano A, Franzese S. Porosity-graded hydroxyapatite ceramics to replace natural bone. Biomaterials. 2001;**22**(11):1365-1370. DOI: 10.1016/S0142-9612(00)00290-8

[26] Sprio S, Ruffini A, Valentini F, D'Alessandro T, Sandri M, Panseri S, et al. Biomimesis and biomorphic transformations: New concepts applied to bone regeneration. Journal of Biotechnology. 2011;**156**(4):347-355. DOI: 10.1016/j.jbiotec.2011.07.034

[27] Dapporto M, Sprio S, Fabbi C, Figallo E, Tampieri A. A novel route for the synthesis of macroporous bioceramics for bone regeneration. Journal of the European Ceramic Society. 2016;**36**(9):2383-2388. DOI: 10.1016/j.jeurceramsoc.2015.10.020

[28] Shah AM, Jung H, Skirboll S. Materials used in cranioplasty: A history and analysis. Neurosurgical Focus. 2014;**36**(4):E19. DOI: 10.3171/2014.2.FOCUS13561

[29] Grant GA, Jolley M, Ellenbogen RG, Roberts TS, Gruss JR, Loeser JD. Failure of autologous bone-assisted cranioplasty following decompressive craniectomy in children and adolescents. Journal of Neurosurgery. 2004;**100**(2 Suppl Pediatrics):163-168. DOI: 10.3171/ped.2004.100.2.0163

[30] Marchac D, Greensmith A. Long-term experience with methylmethacrylate cranioplasty in craniofacial surgery. Journal of Plastic, Reconstructive & Aesthetic Surgery. 2008;**61**(7):744-753. DOI: 10.1016/j.bjps.2007.10.055

[31] Chiarini L, Figurelli S, Pollastri G, Torcia E, Ferrari F, Albanese M, et al. Cranioplasty using acrylic material: A new technical procedure. Journal of Cranio-Maxillofacial Surgery. 2004;**32**(1):5-9. DOI: 10.1016/j.jcms.2003.08.005

[32] Galicich JH, Hovind KH. Stainless steel mesh-acrylic cranioplasty. Technical note. Journal of Neurosurgery. 1967;**27**:376-378. DOI: 10.3171/jns.1967.27.4.0376

[33] Lethaus B, Safi Y, ter Laak-Poort M, Kloss-Brandstätter A, Banki F, Robbenmenke C, et al. Cranioplasty with customized titanium and PEEK implants in a mechanical stress model. Journal of Neurotrauma. 2012;**29**:1077-1083. DOI: 10.1089/neu.2011.1794

[34] Karageorgiou V, Kaplan D. Porosity of 3D biomaterial scaffolds and osteogenesis. Biomaterials. 2005;**26**(27):5474-5491. DOI: 10.1016/j.biomaterials.2005.02.002

[35] Sprio S, Fricia M, Maddalena GF, Nataloni A, Tampieri A. Osteointegration in cranial bone reconstruction: A goal to achieve. Journal of Applied Biomaterials & Functional Materials. 2016;**14**(4):e470-e476. DOI: 10.5301/jabfm.5000293

[36] Sung YM, Shin YK, Ryu JJ. Preparation of hydroxyapatite/zirconia bioceramic nanocomposites for orthopaedic and dental prosthesis applications. Nanotechnology. 2007;**18**(6):65602-65607. DOI: 10.1088/0957-4484/18/6/065602

[37] Sprio S, Tampieri A, Celotti G, Landi E. Development of hydroxyapatite/calcium silicate composites addressed to the design of load-bearing bone scaffolds. Journal of the Mechanical Behavior of Biomedical Materials. 2009;**2**(2):147-155. DOI: 10.1016/j.jmbbm.2008.05.006

[38] Chiba A, Kimura S, Raghukandan K, Morizono Y. Effect of alumina addition on hydroxyapatite biocomposites fabricated by underwater-shock compaction. Materials Science and Engineering: A. 2003;**350**(1):179-183. DOI: 10.1016/S0921-5093(02)00718-9

[39] Li P, Ohtsuki C, Kokubo T, Nakanishi K, Soga N, de Groot K. The role of hydrated silica, titania, and alumina in inducing apatite on implants. Journal of Biomedical Materials Research. 1994;**28**(1):7-15. DOI: 10.1002/jbm.820280103

[40] Kokubo T, Kim HM, Kawashita M. Novel bioactive materials with different mechanical properties. Biomaterials. 2003;**24**(13):2161-2175. DOI: 10.1016/S0142-9612(03)00044-9

[41] Sprio S, Guicciardi S, Dapporto M, Melandri C, Tampieri A. Synthesis and mechanical behavior of b-tricalcium phosphate/titania composites addressed to regeneration of long bone segments. Journal of the Mechanical Behavior of

Biomedical Materials. 2013;**17**:1-10. DOI: 10.1016/j.jmbbm.2012.07.013

[42] Cunha C, Sprio S, Panseri S, Dapporto M, Marcacci M, Tampieri A. High biocompatibility and improved osteogenic potential of novel Ca-P/titania composite scaffolds designed for regeneration of load-bearing segmental bone defects. Journal of Biomedical Material Research Part A. 2013;**101A**:1612-1619. DOI: 10.1002/jbm.a.34479

[43] Cummings SR, Melton LJ. Epidemiology and outcomes of osteoporotic fractures. Lancet. 2002;**359**(9319):1761-1767. DOI: 10.1016/S0140-6736(02)08657-9

[44] Lewis G. Injectable bone cements for use in vertebroplasty and kyphoplasty: State-of-the-art review. Journal of Biomedical Materials Research. 2006;**76B**(2):456-468. DOI: 10.1002/jbm.b.30398

[45] Lewis G. Properties of acrylic bone cement: State of the art review. Journal of Biomedical Materials Research. 1997;**38**(2):155-182. DOI: 10.1002/(SICI)1097-4636(199722)38:2<155::AID-JBM10>3.0.CO;2-C

[46] Boner V, Kuhn P, Mendel T, Gisep A.Temperature evaluation during PMMA screw augmentation in osteoporotic bone—An in vitro study about the risk of thermal necrosis in human femoral heads. Journal of Biomedical Materials Research Part B: Applied Biomaterials. 2009;**90B**(2):842-848. DOI: 10.1002/jbm.b.31353

[47] Friedman CD, Costantino PD, Takagi S, Chow LC. Bone source hydroxyapatite cement: A novel biomaterial for craniofacial skeletal tissue engineering and reconstruction. Journal of Biomedical Materials Research. 1998;**43**(4):428-432.

DOI: 10.1002/(SICI)1097-4636(199824)43:4<428::AID-JBM10>3.0.CO;2-0

[48] Chow LC, Hirayama S, Takagi S, Parry E. Diametral tensile strength and compressive strength of a calcium phosphate cement: Effect of applied pressure. Journal of Biomedical Materials Research. 2000;**53**(5):511-517. DOI: 10.1002/1097-4636(200009)53:5<511::AID-JBM10>3.0.CO;2-E

[49] Bohner M. Reactivity of calcium phosphate cements. Journal of Materials Chemistry. 2007;**17**(38):3980-3986. DOI: 10.1039/b706411j

[50] Bohner M, Gbureck U, Barralet JE. Technological issues for the development of more efficient calcium phosphate bone cements: A critical assessment. Biomaterials. 2005;**26**(33):6423-6429. DOI: 10.1016/j.biomaterials.2005.03.049

[51] Bohner M. Design of ceramic-based cements and putties for bone graft substitution. European Cells & Materials. 2010;**20**:1-12. DOI: 10.22203/eCM.v020a01

[52] Espanol M, Perez RA, Montufar EB, Marichal C, Sacco A, Ginebra MP. Intrinsic porosity of calcium phosphate cements and its significance for drug delivery and tissue engineering applications. Acta Biomaterialia. 2009;**5**(7):2752-2762. DOI: 10.1016/j.actbio.2009.03.011

[53] Zhang J, Liu W, Schnitzler V, Tancret F, Bouler JM. Calcium phosphate cements for bone substitution: Chemistry, handling and mechanical properties. Acta Biomaterialia. 2014;**10**:1035-1049. DOI: 10.1016/j.actbio.2013.11.001

[54] Ishikawa K, Miyamoto Y, Kon M, Nagayama M, Asaoka K. Non-decay type fast-setting calcium phosphate cement: Composite with sodium alginate.

Biomaterials. 1995;**16**(7):527-532. DOI: 10.1016/0142-9612(95)91125-I

[55] Liu W, Zhang J, Weiss P, Tancret F, Bouler JM. The influence of different cellulose ethers on both the handling and mechanical properties of calcium phosphate cements for bone substitution. Acta Biomaterialia. 2013;**9**(3):5740-5750

[56] Alkhraisat MH, Rueda C, Marino FT, Torres J, Jerez LB, Gbureck U, et al. The effect of hyaluronic acid on brushite cement cohesion. Acta Biomaterialia. 2009;**5**:3150-3156. DOI: 10.1016/j.actbio.2012.11.020

[57] Liu H, Li H, Cheng W, Yang Y, Zhu M, Zhou C. Novel injectable calcium phosphate/chitosan composites for bone substitute materials. Acta Biomaterialia. 2006;**2**(5):557-565. DOI: 10.1016/j.actbio.2006.03.007

[58] Wang XP, Chen L, Xiang H, Ye JD. Influence of anti-washout agents on the rheological properties and injectability of a calcium phosphate cement. Journal of Biomedical Materials Research. 2007;**81B**(2):410-418. DOI: 10.1002/jbm.b.30678

[59] Perez RA, Kim HW, Ginebra MP. Polymeric additives to enhance the functional properties of calcium phosphate cements. Journal of Tissue Engineering. 2012;**3**(I):2041731412439555. DOI: 10.1177/2041731412439555

[60] Barinov SM, Komlev VS. Calcium phosphate bone cements. Inorganic Materials. 2011;**47**(13):1470-1485. DOI: 10.1134/S0020168511130024

[61] Sprio S, Tampieri A, Landi E, Sandri M, Martorana S, Celotti G, et al. Physico-chemical properties and solubility behaviour of multi-substituted hydroxyapatite powders containing silicon. Materials Science

and Engineering: C. 2008;**28**(1):179-187. DOI: 10.1016/j.msec.2006.11.009

[62] Marie PJ, Ammann P, Boivin G, Rey C. Mechanisms of action and therapeutic potential of strontium in bone. Calcified Tissue International. 2001;**69**(3):121-129. DOI: 10.1007/s002230010055

[63] Schumacher M, Gelinsky M. Strontium modified calcium phosphate cements—Approaches towards targeted stimulation of bone turnover. Journal of Materials Chemistry B. 2015;**3**: 4626-4640. DOI: 10.1039/c5tb00654f

[64] Montesi M, Panseri S, Dapporto M, Tampieri A, Sprio S. Sr-substituted bone cements direct mesenchymal stem cells, osteoblasts and osteoclasts fate. PLoS One. 2017;**12**(2):e0172100. DOI: 10.1371/journal.pone.0172100

[65] Sprio S, Dapporto M, Montesi M, Panseri S, Lattanzi W, Pola E, et al. Novel osteointegrative Sr-substituted apatitic cements enriched with alginate. Materials. 2016;**9**:763-779. DOI: 10.3390/ma9090763

[66] Amini AR, Laurencin CT, Nukavarapu SP. Bone tissue engineering: Recent advances and challenges. Critical Reviews in Biomedical Engineering. 2012;**40**(5):363-408

[67] Amorosa LF, Lee CH, Aydemir AB, Nizami S, Hsu A, Patel NR, et al. Physiologic load-bearing characteristics of autografts, allografts, and polymer-based scaffolds in a critical sized segmental defect of long bone: An experimental study. International Journal of Nanomedicine. 2013;**8**: 1637-1643. DOI: 10.2147/IJN.S42855

[68] Filardo G, Kon E, Tampieri A, Cabezas-Rodríguez R, Di Martino A, Fini M, et al. New bio-ceramization processes applied to vegetable hierarchical structures for bone

regeneration: An experimental model in sheep. Tissue Engineering. Part A. 2014;**20**(3-4):763-773. DOI: 10.1089/ten. TEA.2013.0108

[69] Tampieri A, Sandri M, Landi E, Pressato D, Francioli S, Quarto R, et al. Design of graded biomimetic osteochondral composite scaffolds. Biomaterials. 2008;**29**(26):3539-3546. DOI: 10.1016/j.biomaterials.2008.05.008

[70] Tampieri A, Celotti G, Landi E, Sandri M, Roveri N, Falini G. Biologically inspired synthesis of bone-like composite: Self-assembled collagen fibers/hydroxyapatite nanocrystals. Journal of Biomedical Materials Research. 2003;**67A**(2): 618-625. DOI: 10.1002/jbm.a.10039

[71] Tampieri A, Sprio S, Sandri M, Valentini F. Mimicking natural bio-mineralization processes: A new tool for osteochondral scaffold development. Trends in Biotechnology. 2017;**29**(10):526-535. DOI: 10.1016/j. tibtech.2011.04.011

[72] Krishnakumar GS, Gostynska N, Campodoni E, Dapporto M, Montesi M, Panseri S, et al. Ribose mediated crosslinking of collagen-hydroxyapatite hybrid scaffolds for bone tissue regeneration using biomimetic strategies. Materials Science and Engineering: C. 2017;**77**:594-605. DOI: 10.1016/j.msec.2017.03.255

[73] Landi E, Tampieri A, Mattioli-Belmonte M, Celotti G, Sandri M, Gigante A, et al. Biomimetic Mg- and $MgCO_3$-substituted hydroxyapatites: Synthesis characterization and in vitro behaviour. Journal of the European Ceramic Society. 2006;**26**(13):2593-2260. DOI: 10.1016/j.jeurceramsoc.2005.06.040

[74] Iafisco M, Ruffini A, Adamiano A, Sprio S, Tampieri A. Biomimetic magnesium-carbonate-apatite nanocrystals endowed with strontium ions as anti-osteoporotic trigger.

Materials Science and Engineering: C. 2014;**35**:212-219. DOI: 10.1016/j. msec.2013.11.009

[75] Ramírez-Rodríguez GB, Delgado-López JM, Iafisco M, Montesi M, Sandri M, Sprio S, et al. Biomimetic mineralization of recombinant collagen type I derived protein to obtain hybrid matrices for bone regeneration. Journal of Structural Biology. 2016;**196**(2):138-146. DOI: 10.1016/j.jsb.2016.06.025

[76] Krishnakumar GS, Gostynska N, Dapporto M, Campodoni E, Montesi M, Panseri S, et al. Evaluation of different crosslinking agents on hybrid biomimetic collagen-hydroxyapatite composites for regenerative medicine. International Journal of Biological Macromolecules. 2018;**106**:739-748. DOI: 10.1016/j.ijbiomac.2017.08.076

[77] Newman AP. Articular cartilage repair. American Journal of Sports Medicine. 1998;**26**(2):309-324. DOI: 10.1177/03635465980260022701

[78] Marcacci M, Kon E, Zaffagnini S, Filardo G, Delcogliano M, Neri MP, et al. Arthroscopic second generation autologous chondrocyte implantation. Knee Surgery, Sports Traumatology, Arthroscopy. 2007;**15**(5):610-619. DOI: 10.1007/s00167-006-0265-9

[79] Bartlett W, Gooding CR, Carrington RWJ, Skinner JA, Briggs TW, Bentley G. Autologous chondrocyte implantation at the knee using a bilayer collagen membrane with bone graft. A preliminary report. Journal of Bone and Joint Surgery. British Volume. 2005;**87**(3):330-332. DOI: 10.1302/0301-620X.87B3.15552

[80] Mano JF, Silva GA, Azevedo HS, Malafaya PB, Sousa RA, Silva SS, et al. Natural origin biodegradable systems in tissue engineering and regenerative medicine: Present status and some moving trends. Journal of the Royal

Society Interface. 2007;**4**(17):999-1030. DOI: 10.1098/rsif.2007.0220

[81] Fedorovich NE, Schuurman W, Wijnberg HM, Prins HJ, van Weeren PR, Malda J, et al. Biofabrication of osteochondral tissue equivalents by printing topologically defined, cell-laden hydrogel scaffolds. Tissue Engineering Part C: Methods. 2012;**18**(1):33-44. DOI: 10.1089/ten. TEC.2011.0060

[82] Gomoll AH, Filardo G, de Girolamo L, Espregueira-Mendes J, Marcacci M, Rodkey WG, et al. Surgical treatment for early osteoarthritis. Part I: Cartilage repair procedures. Knee Surgery, Sports Traumatology, Arthroscopy. 2012;**20**:450-466. DOI: 10.1007/s00167-011-1780-x

[83] Filardo G, Perdisa F, Gelinsky M, Despang F, Fini M, Marcacci M, et al. Novel alginate biphasic scaffold for osteochondral regeneration: An in vivo evaluation in rabbit and sheep models. Journal of Materials Science: Materials in Medicine. 2018;**29**(6):74. DOI: 10.1007/s10856-018-6074-0

[84] Sherwood JK, Riley SL, Palazzolo R, Brown SC, Monkhouse DC, Coates M, et al. A three-dimensional osteochondral composite scaffold for articular cartilage repair. Biomaterials. 2002;**23**(24):4739-4751. DOI: 10.1016/S0142-9612(02)00223-5

[85] Filardo G, Kon E, Perdisa F, Di Matteo B, Di Martino A, Iacono F, et al. Osteochondral scaffold reconstruction for complex knee lesions: A comparative evaluation. The Knee. 2013;**20**(6):570-576. DOI: 10.1016/j.knee.2013.05.007

[86] Marcacci M, Zaffagnini S, Kon E, Marcheggiani Muccioli GM, Di Martino A, Di Matteo B, et al. Unicompartmental osteoarthritis: An integrated biomechanical and biological approach as alternative

to metal resurfacing. Knee Surgery, Sports Traumatology, Arthroscopy. 2013;**21**(11):2509-2517. DOI: 10.1007/s00167-013-2388-0

[87] Sprio S, Sandri M, Panseri S, Cunha C, Tampieri A. Hybrid scaffolds for tissue regeneration: Chemotaxis and physical confinement as sources of biomimesis. Journal of Nanomaterials. 2012;**2012**:418281. DOI: 10.1155/2012/418281

[88] Kon E, Delcogliano M, Filardo G, Fini M, Giavaresi G, Francioli S, et al. Orderly osteochondral regeneration in a sheep model using a novel nano-composite multilayered biomaterial. Journal of Orthopaedic Research. 2010;**28**(1):116-124. DOI: 10.1002/jor.20958

[89] Hoemann CD, Hurtig M, Rossomacha E, Sun J, Chevrier A, Shive M, et al. Chitosan-glycerol phosphate/blood implants improve hyaline cartilage repair in ovine microfracture defects. Journal of Bone and Joint Surgery. American Volume. 2005;**87**(12):2671-2686. DOI: 10.2106/JBJS.D.02536

[90] Pavalko FM, Norvell SM, Burr DB, Turner CH, Duncan RL, Bidwell JP. A model for mechanotransduction in bone cells: The load-bearing mechanosomes. Journal of Cellular Biochemistry. 2003;**88**(1):104-112. DOI: 10.1002/jcb.10284

[91] Lucas PW, Darvell BW, Lee PKD, Yuen TDB, Choong MF. The toughness of plant cell walls. Philosophical Transactions of The Royal Society B. Biological Sciences. 1995;**348**(1325):363-372. DOI: 10.1098/rstb.1995.0074

[92] Greil P, Lifka T, Kaindl A. Biomorphic cellular silicon carbide ceramics from wood: I. Processing and microstructure. Journal of the European Ceramic Society. 1998;**18**(14):1961-1973. DOI: 10.1016/S0955-2219(98)00156-3

[93] Greil P, Lifka T, Kaindl A. Biomorphic cellular silicon carbide ceramics from wood: II. Mechanical properties. Journal of the European Ceramic Society. 1998;**18**(14):1975-1983. DOI: 10.1016/S0955-2219(98)00155-1

[94] de Arellano-López AR, Martínez-Fernández J, González P, Domínguez C, Fernández-Quero V, Singh M. Biomorphic SiC: A new engineering ceramic material. International Journal of Applied Ceramic Technology. 2004;**1**(1):56-67. DOI: 10.1111/j.1744-7402.2004.tb00155.x

[95] Rambo CR, Sieber H. Novel synthetic route to biomorphic Al_2O_3 ceramics. Advanced Materials. 2005;**17**(8):1088-1091. DOI: 10.1002/adma.200401049

[96] Ruffini A, Sprio S, Tampieri A. Study of the hydrothermal transformation of wood-derived calcium carbonate into 3D hierarchically organized hydroxyapatite. Chemical Engineering Journal. 2013;**217**:150-158. DOI: 10.1016/j.cej.2012.11.107

Applications of Electrokinetics and Dielectrophoresis on Designing Chip-Based Disease Diagnostic Platforms

*Ezekiel O. Adekanmbi and Soumya K. Srivastava*

Abstract

This chapter discusses the concepts of electrokinetics, dielectrophoresis and how they intertwine with other forces in microsystems to aid microfluidic disease diagnostics. Methods of obtaining the intrinsic electrical properties of biological materials are first discussed alongside the mechanisms governing the variations in the intrinsic properties when biological entities become diseased/infected. The procedure and importance of modeling and simulation of disease detection platforms prior to their fabrication and testing is also discussed. Fabrication techniques for low- and high-resource settings are presented as well. The various applications of the synergy of dielectrophoresis and electrokinetics for disease detection are discussed. The chapter will end with some novel ideas about the believed future directions of the electrokinetic methods for early, intermediate, and late-stage disease detection either as adjuncts of various existing diagnostic methodologies or as a stand-alone diagnostic alternative.

Keywords: electrokinetics, dielectrophoresis, microsystems, disease diagnostics, dielectric properties

1. Introduction

Electrokinetics (EK), as the name implies, is a technique of using electric field to cause motion. The motion can be that of a liquid or colloidal particle (microscopic solid particles suspended in a fluid). This concept of electrokinetics has four main features: Electro-osmosis (EO), electrophoresis (EP), streaming potential (StP), and sedimentation potential (SeP). In the disease diagnostics arena—an integral part of the application of microfluidics in healthcare, electro-osmosis and electrophoresis are the main electrokinetic forces that particles experience. Electro-osmosis involves the bulk motion of a liquid through a solid surface under the influence of electric field. On the other hand, electrophoresis is the motion of a solid material through a liquid under an electric field effect. Both electrophoresis and electro-osmosis require that the surface of the solid be charged. As shown in **Figure 1**, when the surface of the particle, placed within a uniformly distributed electric field, is positively charged (A), the particle (suspended in a characterized liquid) moves to the left but to the right (against the field direction) when the charge on the surface
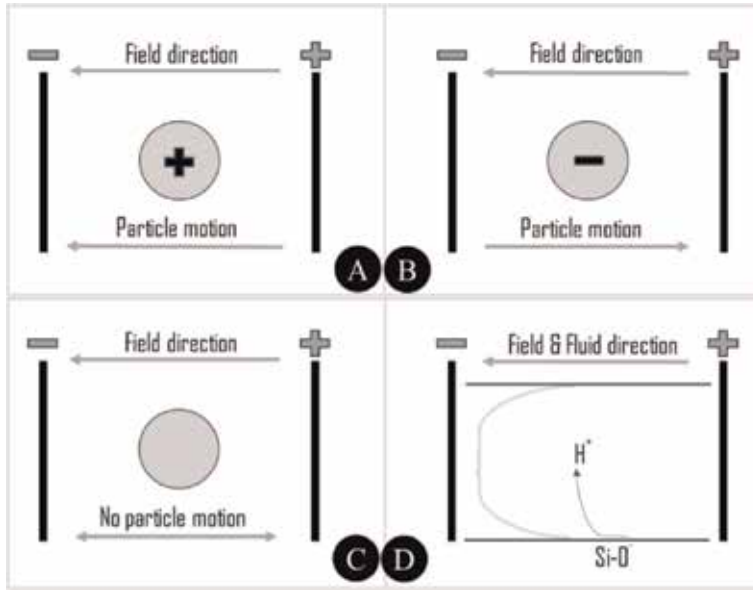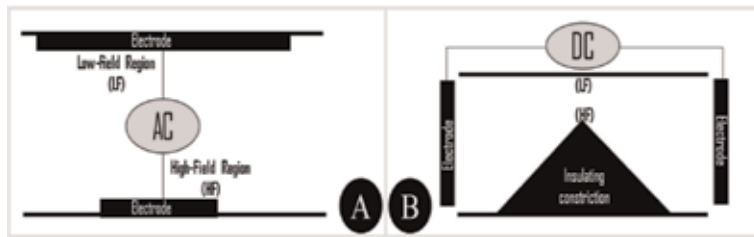
Figure 1.
The representation of electro-osmosis and electrophoresis as the two main electrokinetic phenomena in microfluidic channels: (A) positively charged particle under a uniform field region effect will move toward the negative electrode according to the fundamental attraction-repulsion laws. (B) Negatively charged particle placed under the same electric field region will migrate toward the positive electrode. (C) A no-charge (neutral) particle placed in the same field region will experience no electrophoretic motion because electrophoresis only applies to charged particles. (D) Representation of the deprotonation of the terminal (SiOH)/surface chemical group of the channel wall (treated poly(dimethyl siloxane) (PDMS) or uncoated glass), which births the electro-osmotic pumping within the channel.

is reversed (B). If the particle is a neutral body (C), no electrophoretic effect will be seen. **Figure 1D** is a case where liquid is flowing through a charged solid surface. The solid surface (usually glass or surface-treated polymer) become deprotonated when in contact with the liquid such that counter (positive) ions from the liquid goes into the channel surface to firmly replace the detached positive ions forming what is referred to as the Stern layer. Columbic force of attraction causes the Stern layer to, in turn, attract negative ions from the liquid forming the diffuse layer (together with some unattached positive charges) beyond which the region of electro-neutrality is initiated. A plane, called the slipping plane, formed around the loosely-bound diffuse layer is very crucial to how the bulk of the liquid would move when the electric field if applied across the static upstream and downstream flow region. The potential of this slipping plane is called the Zeta potential, ζ [1]. The same concept of Zeta potential applies to a charged solid moving through a liquid. For a charged solid moving through a liquid under an electric field effect, the rate of motion of the solid, r_{ep}, depends on the Zeta potential at its slipping plane, ζ_p, viscosity of the liquid in which it is moving, η, dielectric constant of the liquid, ε_m, as well as the strength of the applied electric field, E. Mathematically, this has been represented as

$$r_{ep} = f\left(\zeta_p, \varepsilon_m, \eta, E\right) = \left(\zeta_p \varepsilon_m E\right)/\eta \tag{1}$$

On the other hand, when a liquid is flowing through a charged wall of Zeta potential, ζ_w, the positional rate of flow of the liquid, r_{eo}, is given by

$$r_{eo} = f(\zeta_w, \varepsilon_m, \eta, E) = -\zeta_w \varepsilon_m E)/\eta \tag{2}$$

Figure 2.
Generation of non-uniform electric fields for dielectrophoretic applications; (A) simple unequal spatial electrode-pair arrangement connected to an AC source with the lower electrode acting as the high-field region while the upper electrode on the low-field region. The field low-high regions remain the same even when the electrode terminals are interchanged owing the frequency component of the AC source (B) insulating constriction (or obstacle) changed the uniform field between the electrodes to non-uniform field at its location.

In dielectrophoresis (DEP), the applied electric field must be non-uniform. The movement of the particles in non-uniform electric field does not depend primarily on the particle charge but on the ability of the particle to become polarized relative to that of the suspending medium [2].

Therefore, DEP force is always in effect when the particle is charged or not. This means, dielectrophoresis, therefore, safely be defined as a technique of using non-uniform electric field to induce the motion of a charged or an uncharged particle. Electric field can be rendered non-uniform in different ways. **Figure 2** shows some examples of how to generate non-uniform electric fields using AC or DC source. For the AC field, a simple unequal spatial electrode-pair arrangement (**Figure 2A**) would generate non-uniform field (AC DEP or classical DEP). A second method is to place an insulating constriction within a simple straight channel operating under DC condition that would make the field non-uniform (DC-iDEP or iDEP). There is never any hard and fast rule regarding how the electrodes should be arranged or the constrictions be distributed but simulation could assist in formulation of the device architecture. Every researcher has a purpose in mind and that purpose drives the architecture of the channel or device without denying the underlining physics.

2. Characterization of biological cells

Characterization of biological entities like cells involves the utilization of various methods including but not limited to electrical, magnetic, acoustic, and optical characterization to explore cell properties. In this section, electrical method will be discussed (with focus on dielectrophoresis) since dielectrophoretic force is related, in part, to the electrical properties of the biological cell. In the utilization of electrical method for bioparticle characterization, it is not uncommon to use impedance cytometry, dielectrophoresis, and electrorotation. Impedance cytometry works on the principle that when a particle suspended in a conductive fluid passes through a small orifice (comparable to the size of the particle) created by two electrodes, the passage of the particle through the (usually AC) electric field between the electrodes results in the generation of electric signal, which can be processed to provide valuable information about the electrical properties of the particle. In electrorotation, four electrodes are each charged with AC voltage of different phases to generate a rotating electric field, thus setting up an electrical torque. When a (spherical) particle is placed within this rotating field, it becomes polarized inducing a dipole. The dipole moment induced within this particle rotates with the electric field at certain velocity. However, the multiphase nature of the four electrodes causes the particle to lag behind the field by a factor that depends on the

frequency of the rotating field. Since the particle velocity is determined by the torque in the rotating electric field, electrical properties of the particle can be extracted measuring the dependence of the torque on the field frequency. With dielectrophoresis, the case is different. When a charged or uncharged spherical particle is placed between an unequally dimensioned AC electrode-pair which is generating non-uniform electric field, (**Figure 2A**) the particle becomes polarized just as the medium in which the particle is suspended [3]. The particle could then move toward the region of high field (HF), low field (LF) or remain unperturbed by the field depending on the properties of the applied electric field, suspending medium and the particle itself. When the particle moves toward the HF region, the phenomenon is termed positive dielectrophoresis (pDEP) while it is called negative dielectrophoresis (nDEP) if the particle's translational motion is toward the LF region [4]. Usually, when a particle is experiencing nDEP, for instance, it does so over a range of frequency. As the frequency changes further, the particle can translate to the pDEP regime. Before this happens, however, at a specific point of inflection where the particle comes to a halt before changing regime must have been reached. The frequency at such point of inflection is termed crossover frequency. At the crossover frequency i.e. after the application of the AC electric field parameters, the particle is only vibrating at a spot without any appreciable translational motion. At this point, the particle experiences no DEP force (F_{DEP} = 0).

$$F_{DEP} = 2\pi r^3 \varepsilon_0 \varepsilon_m Re\left[f_{CM}\right]\nabla E^2 = 0 \tag{3}$$

where $f_{CM} = \frac{\varepsilon_p^* - \varepsilon_m^*}{\varepsilon_p^* + 2\varepsilon_m^*}$ connecting both permittivity and conductivity (electrical properties) of both the particle (ε_p, σ_p) and its suspending medium (ε_m, σ_m) respectively.

This implies that the real part of the Clausius-Mossotti (CM) factor, $Re\left[f_{CM}\right] = 0$.

That is, $Re\left(\frac{\varepsilon_p^* - \varepsilon_m^*}{\varepsilon_p^* + 2\varepsilon_m^*}\right) = 0$ where $\varepsilon_i^* = \varepsilon_i - j\frac{\sigma_i}{\omega}$

Hence, $Re\left[\frac{\left(\varepsilon_p - j\frac{\sigma_p}{\omega}\right) - \left(\varepsilon_m - j\frac{\sigma_m}{\omega}\right)}{\left(\varepsilon_p - j\frac{\sigma_p}{\omega}\right) + 2\left(\varepsilon_m - j\frac{\sigma_m}{\omega}\right)}\right] = 0$

$$Re\left[\frac{\left(\varepsilon_p - j\frac{\sigma_p}{\omega}\right) - \left(\varepsilon_m - j\frac{m}{\omega}\right)}{\left(\varepsilon_p - j\frac{\sigma_p}{\omega}\right) + 2\left(\varepsilon_m - j\frac{\sigma_m}{\omega}\right)} \ x \ \frac{\left(\varepsilon_p - j\frac{\sigma_p}{\omega}\right) + 2\left(\varepsilon_m - j\frac{\sigma_m}{\omega}\right)}{\left(\varepsilon_p - j\frac{\sigma_p}{\omega}\right) + 2\left(\varepsilon_m - j\frac{\sigma_m}{\omega}\right)}\right] = 0 \tag{4}$$
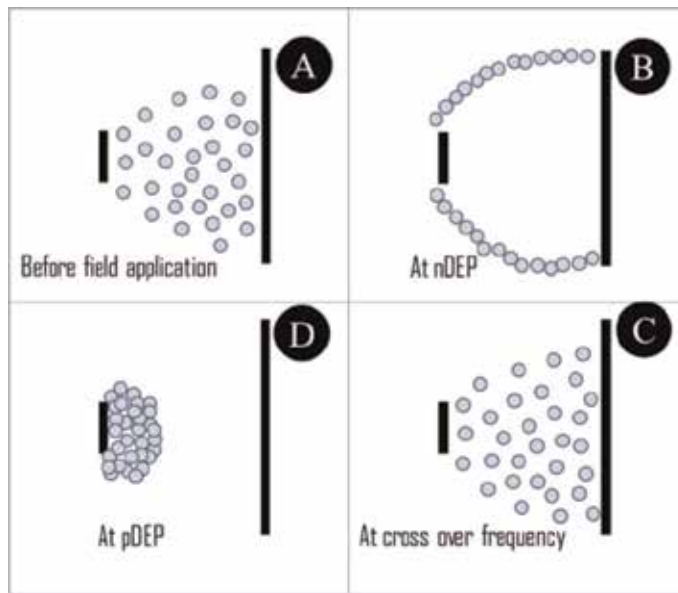
$$Re\left[\left(\varepsilon_p - j\frac{\sigma_p}{\omega}\right) - \left(\varepsilon_m - j\frac{m}{\omega}\right)\right]\left[\left(\varepsilon_p - j\frac{\sigma_p}{\omega}\right) + 2\left(\varepsilon_m - j\frac{\sigma_m}{\omega}\right)\right] = 0 \tag{5}$$

$$\varepsilon_p^2 + \varepsilon_m\varepsilon_p - j\frac{\varepsilon_p\sigma_p}{\omega} - 2j\frac{\varepsilon_p\sigma_m}{\omega} - 2\varepsilon_m^2 + j\frac{\varepsilon_m\sigma_p}{\omega} + 2j\frac{\varepsilon_m\sigma_m}{\omega} + j\frac{\varepsilon_p\left(\sigma_m - \sigma_p\right)}{\omega}$$
$$+ 2j\frac{\varepsilon_m\left(\sigma_m - \sigma_p\right)}{\omega} - j^2\frac{\sigma_p\left(\sigma_m - \sigma_p\right)}{\omega^2} - 2j^2\frac{\sigma_m\left(\sigma_m - \sigma_p\right)}{\omega^2} = 0 \tag{6}$$

Setting the real part to zero with $j^2 = -1$ gives $\varepsilon_p^2 + \varepsilon_m\varepsilon_p - 2\varepsilon_m^2 + \frac{\sigma_p\left(\sigma_m - \sigma_p\right)}{\omega^2} + 2\frac{\sigma_m\left(\sigma_m - \sigma_p\right)}{\omega^2} = 0$, $\exists \ \omega = 2\pi f_{co}$ with f_{co} as the crossover frequency, then using the identity; $a^2 + ab - 2b^2 = (a - b)(a + 2b)$, we can rearrange to obtain f_{co} as

$$f_{co} = \frac{1}{2\pi}\sqrt{\frac{\left(\sigma_p - \sigma_m\right)\left(\sigma_p + 2\sigma_m\right)}{\left(\varepsilon_p - \varepsilon_m\right)\left(\varepsilon_p + 2\varepsilon_m\right)}} \tag{7}$$

Figure 3.
Images of the particle behavior under different field frequencies. (A) Particles well dispersed before field application. (B) Particles undergoing nDEP forming chains with increased particle-particle interaction. (C) Particles at cross over frequency; no response to the dielectrophoretic force. (D) Particles clinging to the high-field region depicting pDEP.

Eq. (7) represents a simplified presentation of the first crossover frequency (f_{co}) of a particle in relation to the permittivity and conductivity (electrical properties) of both the particle (ε_p, σ_p) and its suspending medium (ε_m, σ_m) respectively. To extract the electrical properties of the particle, it is common to obtain a data set comprising of varied medium conductivity and hence, varied crossover frequency.

The conductivity-frequency data is then fitted with the appropriate model representing the biological materials of interest. Human red blood cells (RBCs), for instance, can be modeled as a bag of cytoplasm have an insulating plasma membrane. This type of model is popularly referred to as the single-shell model [5, 6]. **Figure 3A** shows the representative images of nDEP, pDEP, and crossover states for RBCs at a given AC amplitude and sweeping frequencies. Experiments resulting in these images are generally conducted by suspending the particles in an isotonic medium (5% dextrose and fed into a reservoir sealed onto a borosilicate glass with an interfacial 90°, low-separation electrode-pair connected to an arbitrary wave-form generator. At a fixed amplitude output, the frequency of the AC field was varied until the crossover frequency was reached and surpassed. The conductivity of the suspending medium was then sequentially increased using phosphate-buffered saline (PBS) or other conductivity conditioners and at each increase, the corresponding crossover frequency was obtained. For other bioparticles such as the nucleated white blood cells and bacteria, the double-shell and three-shell models can be applied respectively. Detailed shell analysis for biological cells is available in diverse literatures [7–10].

3. Modeling and simulation of microdevices

The popularity of six sigma DMAIC (define, measure, analyze, improve, and control) approach has made more companies to embrace extensive modeling and

simulation in order to save cost and time. In the production of chip-based disease diagnostic platforms, numerical computation is seen as an important process step as it affords the flexibility of exploring how various parameters affect device performance without the need for extensive experimental research. In cases where experimental activities are needed to improve numerical computations, the utilization of the design of experiment principles is usually a wise choice. In the design of experimental principles, ability to obtained related factors, which can be confounded optimally is a key component of the cost and time-saving strategy. Microfluidic devices for disease diagnostics can be operated using AC or DC sources. Discussion in this section will be based on DC operations. Details of AC-operated designs have been given elsewhere [11–13].

In DC models for disease diagnostics, electro-osmosis and dielectrophoresis are usually the electrokinetic mechanism that governs the transport phenomena prior to the region of electric field non-uniformity within the channel [14]. At the region of non-uniform electric field, the dielectrophoretic force is combined with these electrokinetic forces to bring about the desired particle differentiation either through trapping (pDEP) or streaming (nDEP). A smart idea, then, is to locate the exit channels close to the region immediately following the field gradient so that sorted bioparticles can be collected appropriately. Failure to do this might result in the recombination of streamlines, which tend to restore the separated cells to their ab initio states.

Models of the envisaged diagnostic devices are usually drawn to scale using any suitable software. (AutoCAD, SolidWorks, *etc.*). These models are then interfaced with multi-physics simulation software such as COMSOL Multiphysics, FLUENT, to explore parameter dependence and their effects of targeted outcomes. It is not uncommon to draw the models using the functionalities available in the simulation software themselves. One requirement to emphasize here is the sound knowledge of the physics governing the operations of the diagnostic device. These inexhaustible physics are discussed in this section. For insulator-based (iDEP) diagnostic devices, the physics usually involve momentum transport (Newton's Law), mass transport (Fick's Law), energy transport (Fourier's Law) and charge transport (Maxwell's Laws/Ohm's law) [15].

Momentum transport involves the transfer of momentum from one particle to another. This transfer results in the continuous change in fluid's positional space leading to the concept of fluid dynamics (hydrodynamics for liquids). Depending of the focus of any project, momentum transport can be explored in 1D, 2D or 3D. One good approximation in iDEP devices is that the complexity of 3D consideration can be avoided by using 2D analysis provided the channel's width-to-depth ratio is about 5:1. The 3D to 2D approximation is also good on the basis that turbulence is not a common occurrence in micron-sized devices. The governing equations for momentum transport are generally the Navier-Stokes and mass continuity equations [16] (Eqs. 8 and 9). Navier-Stokes equation is usually reduced to Stokes equation when the continuity equation is applied at static conditions under the assumption that the Reynolds number is very low. This makes the computer solve, numerically, for the pressure and velocity distributions within the channel. Prior to obtaining the pressure and velocity profiles, appropriation boundary conditions are utilized to completely define the system. In iDEP operations, electroosmotic wall is specified in lieu of the 'no-slip' wall condition. This is because, in electro-osmotic flow, the bulk motion of the fluid is driven by the wall effects - a phenomenon termed electro-osmotic pumping. Electro-osmotic pumping makes the use of external pumping mechanism unnecessary. The boundary mainly utilizes the electric field solution obtained from the second physics (electric current node in, for instance, COMSOL Multiphysics) which is usually solved together with the fluid

flow equations in stationary mode. The electric current module requires that the electric potential be specified in addition to electrical insulating boundaries. The spatial distribution of the electric field strength with the channel reveals that when constrictions are placed within a uniform microchannel, the effect is non-uniformity in field strength. This non-uniformity is usually seen using, in COMSOL Multiphysics for instance, color pallet or legend. As theory suggests, dielectro-phoretic force acts only at the region with field gradient (i.e. at the constriction(s)). Suffice it to say that the solved electric current equations in iDEP systems usually include Ohm's law, electric displacement and the charge conservation.

After solving the fluid and electric current equations in stationary mode to obtain the distributions of velocity, pressure and electric field within the diagnostic device, it is expedient to visually and quantitatively verify if the sorting or trapping process results in the desired output. Two approaches are possible; (1) using Fick's law of diffusion to classify the components of the mixture as unique tubes through the transport of diluted species module or (2) using a balance of viscous drag and dielectrophoretic force through particle tracking module. In the former, it is expected that the concentration gradient between the inlet and the outlet ports may cause diffusion and when the electro-osmotic flow is initiated for bulk fluid motion, convective flux also comes into play. This implies that the total particle flux can be expressed as the sum of diffusive, EP, DEP and convective flux:

$$N_i = -D_i \nabla c_i + \left(u + \mu_{EP,i} + \mu_{DEP,i} \nabla E^2\right) c_i \tag{8}$$

and

$$\frac{\partial c_i}{\partial t} + \nabla . N_i = R_i \tag{9}$$

where $\vec{u}$ is the hydrodynamic velocity vector, D_i is the diffusivity of the particle, $\vec{E}$ is the electric field applied, and μ_{EP} and μ_{EP} are the EP and DEP motilities respectively. The DEP mobility is a function of CM factor and for a spherical particle it is expressed as:

$$\mu_{DEP} = \frac{\pi d_p^2 \varepsilon_m}{12\eta} f_{CM} \tag{10}$$

where d_p is the particle diameter and η is the medium viscosity. In the latter, the drag force is given as; $F_{drag} = \frac{9\eta}{2\rho_p r_p^2} m_p(u - v)$ which is balanced with the DEP equation (Eq. 3).

4. Microdevice fabrication

Microdevice fabrication has traditionally been through the lithographic and etching process. In iDEP devices constructed with polymer, a combination of lithography, etching and rapid prototyping is usually utilized. While lithography prints the patterns on the substrates (glass or silicon wafers), etching creates the grooves on those patterns and rapid prototyping transfers the substrates patterns to polymer. The lithography process starts with the printing of the patterns made in the modeling and simulation stage. Usually, the patterns assisted by laser or electron-beam (and other process steps) are printed on a transparent-opaque pair plate which could further transfer the printed patterns to a resist-coated substrate in

the next stage of the microfabrication process. The plate is transparent where light is desired to pass but opaque where it is undesirable. This transparent-opaque pair plate is referred to as photomask. The architecture of the photomasks determines the final patterns (convex or concave, depending on the type of photoresist used) on the substrates after photoresist development, depending on the type of photoresist on the substrate. **Figure 4** shows the two forms of photomasks commonly used in iDEP device making process.

Details of the process steps involved in photomask printing have been given by Mack [17]. One important point to note is that mask making process is probably the most important step in microfabrication. Any error associated with dimensions during this mask-making process will propagate through the whole microfabrication process. In iDEP devices, all dimensions (especially at the constrictions regions) are critical. A change in the fillet angle, for instance, can affect the gradient of the electric field within the device and this could, in turn, change the efficiency of the device. Following the mask-making process is the cleaning of substrates onto which the mask patterns will be transferred. Cleaning substrate can be achieved through chemical (acetone, ethanol) or physicochemical (plasma cleaning) means. In some cases, cleansed substrates are treated with adhesion promoting agents such as silane, organotitanates, organozirconates and their derivatives. These coupling agents tend to act as binders between the substrates and the photoresist. Depending on whether concave or convex patterns are desired, positive or negative photoresists are spin-coated on the cleansed substrates at some pre-determined spin coating parameters to ensure uniform surface roughness and film thickness and prevent speckle or void formation. Following the spin coating process is the low-temperature baking step. This is the step that removes some of the solvent in the resist itself. Lowering the solvent content of the film is essential to preserve its integrity at room temperature since moisture content of the film could change the film properties, enhance contamination and thus damage the entire lithographic process. It is important to note that this baking step, which tend to lower the moisture content of the film, could reduce film thickness. It is therefore expedient to factor this effect into consideration when quantifying the resist volume and spin coating parameters prior to coating. A pre-baked resist-coated substrate is ready for UV exposure after the photomask has been correctly aligned with its positional space to circumvent any overlay. The dosing period of the UV depends, amongst other factors, on its intensity, the type, and percentage composition of the photoactive component of the resists. Usually, photoresists manufacturers provide the guidelines for UV exposure using certain substrate (usually silicon-based). Using a different substrate from the manufacturers' test substrate might have its own effect on the critical dimensions of the microstructure. If positive photoresist is used (together with mask A in **Figure 4**), it is expected that the exposed region will be less soluble owing to the change in the chemistry of the resist after exposure to ultraviolet (UV) light. Post-exposure baking and development of the resist will create the pattern vials which act as guides for the etchants during the etching

Figure 4.
Different forms of mask used in photolithography. (A) The mask intend for positive substrate photoresist and (B) the mask for negative photoresist.

process. After UV exposure, the substrate is usually baked to create a final structure that would reduce undercut and improve selectivity during the etching process. After this post UV-exposure baking, the resist is developed to remove the part of the resist that have been weakened by the UV. Another type of resist called chemically amplified resist has also become more common. This resist is not weakened or hardened by the photo exposure. Rather, it generates some form of cationic entity that becomes amplified during the post exposure baking and thus makes development meaningful. As mentioned earlier, the structural integrity of lithographic features is partly a function of the UV dosage. Over exposure and under exposure should be avoided. After the resist development stage, it is important to conduct some form of metrology to verify the conformance of critical dimensions and check if any overlay has occurred because of substrate relocation or displacement during mask alignment. Critical Dimension-SEM is probably the best metrological undertaking. As much as possible, the use of laser profiling system should be avoided as the collimated laser tend to form unwanted patterns on the resist. Once the dimensions of the features have been verified and defects such as edge effects have been substantially avoided/minimized, the substrate is then moved to the etching phase. Etching is the removal of some parts of the substrate as guided by the resist patterns. There are two main types of resist: Dry and Wet. Wet etching usually in HF or its mixture with HNO_3, i.e., HF/HNO_3 mixture has been traditionally used as etchant. However, with the Moore's law becoming obsolete and lithographic features turning smaller day by day, dry/plasma etching are becoming preferable. After etching, some metrological analysis could also be made to check the efficiency of the etching process. Once the etched substrate has been certified okay, the next stage is the transfer of the etched patterns to the polymer. In iDEP devices, several polymers can be used for the patterning, but silicone elastomer (PDMS) seems to be more widely accepted. By mixing silicone with its curing agent in the prescribed ratio (10:1), an air-ridden mixture whose air component can be removed through vacuum-degassing operation in any closed container is formed. Degassed mixture could then be poured onto the etched substrate (herein referred to as the master), cured thermally or at ambient conditions and systematically peeled off the master, diced, punched and completed with electrodes for dielectrophoretic experiments. Depending on the goal of the researcher, external devices such as syringe pump, microsensors, imaging line, *etc.* can be attached to the iDEP device. The completion of the device fabrication stage is the hydrophobic ceiling of the cured PDMS to glass or other PDMS material. PDMS is known to be hydrophobic owing to its terminal $Si-O-CH_3$ bond. This terminal bond will prevent wall-surface ionization which is necessary to initiate electrodynamic flow within the channel. There are several ways to treat this hydrophobic wall in order to render it hydrophilic by changing the $Si-O-CH_3$ bond to $Si-O-H$. One common way is plasma oxidation. The plasma oxidation process involves using the radio frequency (RF) generated by changing magnetic field under low-pressure and certain gas to produce plasma, which is a mixture of electrons, atoms, molecules and other components depending on the nature of the gas used. It is believed that certain component of the plasma is responsible for the surface reaction which replaced $-OCH_3$ with OH terminal. After surface treatment, high surface energy of the PDMS allows its bonding to glass/other treated PDMS and also prevents the suspending medium from beading up within the microfluidic channel thus preventing air bubbles from being trapped. To ensure that the sealing is perfect (i.e. the sealing is leak proof), the sealed reservoir can be filled with deionized water and anhydrous copper sulfate spread around the sealed interface. The whole set up is then placed in a controlled environment for confirmatory test. If the white color of the sulfate turns blue at the end of the test period, then sealing is not leak-free, and the device should be discarded.

It is important to do this check because leaking device would lead to an untold operation error since the leakage will induce pressure gradient which will belie the desired electro-osmotic flow within the channel.

5. Disease detection

Sections 1–3 have detailed how bioparticles can be characterized, iDEP devices modeled/simulated and how the numerically obtained device architecture can be fabricated using lithography and transferred to polymer using prototyping. This section will focus more on testing the fabricated devices and comparing its efficiency with the numerically obtained one. The experimental process of disease detection using iDEP devices starts with preparation of the bioparticles for DEP experiment. In some cases, the bioparticles of interests are cultured while in other cases, they are obtained and tested directly from donors, stored temporarily and worked on. Several other methods exist for obtaining samples. Irrespective of the method of obtaining the bioparticle samples, one important factor to consider before experimentation is the properties of the suspending medium. It is customary in iDEP experimentations to suspend bioparticles in a medium prior to feeding them into the inlet reservoir. During the operation of the iDEP device, it is necessary to prevent Joule heating or electrolysis in the iDEP devices by using low-conducting medium. Preventing Joule heating circumvents, amongst other things, any form of recirculation within the channel especially at the post-constriction regions [7]. Knowing that cells are cultured in relatively conducting medium at pH range that depends on the nature of the bioparticles, it is necessary to pre-treat the samples and make them fit for dielectrophoretic experimentation. The pH value of the suspending medium affects the Zeta potential of the bioparticle as well as that of the iDEP channel wall. These will in turn affect the electro-osmotic and electrophoretic contributions to the flux of particles within the channel. Apart from the medium pH, its tonicity (which is related to its osmolality) is also important. A hypertonic medium causes plasmolysis while a hypotonic result in cell turgidity. According to Eq. 3, the dielectrophoretic force experience by bioparticles depends, amongst other factors, on the size of the particle. If the suspending medium is hypertonic, it results in an increased particle radius whose effect on the DEP force is to the third power. Reduction in particle radius when the particles are suspended in a hypotonic solution has a reversed effect on the DEP force. For this reason, isotonic solution may be the more appropriate medium for preserving the cell size since there is no net movement of fluid when the cells are suspended. 5% dextrose and 0.9% NaCl are considered isotonic medium and are therefore good choices for iDEP experiments. Using direct current (DC) to generate electric field for iDEP experiment requires that one leverage the membrane characteristics of the bio-particles in context. This is because DC manipulation of cells cares less about the variation in field frequency which is the main factor in AC fields (higher AC frequency tends to put cytoplasmic contributions into account). According to the complex permittivity relation, $\tilde{\varepsilon}_i = \varepsilon_i - j\frac{\sigma_i}{\omega}$, the first term on the right represents, for a cell membrane, the polarization component of the dielectric (membrane) while the second component represent the dielectric loss component. Since DC and low-frequency AC fields seem to be comparable in terms of their effects on biological cells, it is expected that dielectric loss might be an issue. Primarily, a healthy cell has a membrane that separates its intercellular contents from its outer environment. Situated within the membrane are channels that allow certain ions to be exchanged between the internal and external environment of the cell depending on their concentrations on either side of the membrane. The disparity in the concentration-pair results in

membrane potential which is usually maintained as resting membrane potential through ion leakage and pumping. This potential difference places certain capacitance on the membrane relative to the charges associated with both sides of the membrane. At the onset of infection (intracellular infection, for instance), the damage to the membrane causes excessive ion change, which results in a change in the capacitance of the membrane. If the infection had engendered some proteins to be expressed on the cell membrane, that would have disrupted the charge distribution on the external environment contiguous to the membrane resulting in a different membrane capacitance. This difference is enough to make healthy and infected move into different paths when placed in a dielectrophoretic micro channel [18]. When infected and healthy cells move to diverse exit ports, they can be easily quantified and/or qualified. Common qualification technique involves post separation microscopic evaluation. This might involve cell staining and fluorescence characterization. In some cases, post separation qualification is achieved by integrating sensors i.e. measuring impedance or capacitance along the exit channels. These sensors work in a similar fashion to impedance cytometry. When separated a particle passes through the gap between the sensor, spectra are generated from where the nature of the particle is verified and compared with any baseline spectra. For identifying extracellular infection in human blood, for instance, there is a need to primarily isolate the blood plasma and then explore the possibility of singling out the pathogen. Lyme disease is best detected this way, but the process can be very challenging due to the complexity of the plasma component.

6. The future of dielectrophoresis

Having walked through the essential steps involved in the design, fabrication and testing of iDEP disease diagnostic device, a very pertinent question remains: where is this dielectrophoretic analysis heading to? iDEP is currently the choicest dielectrophoretic methodology for bioparticle separation/disease diagnostic purposes. This method could still be classified as being in the teething stage going by the number of research work that are published, especially since 1992. Therefore, iDEP is poised do more than separation and detection of bioparticle. For instance, bioparticle are currently being characterized using electrode-based (AC) dielectrophoresis. iDEP can be used to replace this age-long method through directional etching of glass substrate. This will boost the expansion of AC-DC DEP for simultaneous particle characterization, separation and detection. On glass, groove can be etched systematically and conducting metals, such as copper, can be electrochemically deposited.

Acknowledgements

Conflict of interest

The authors declare no conflict of interest.

Author details

Ezekiel O. Adekanmbi and Soumya K. Srivastava*
Department of Chemical and Materials Engineering, University of Idaho, USA

*Address all correspondence to: srivastavask@uidaho.edu

IntechOpen

References

[1] Kirby BJ. Micro- and Nanoscale Fluid Mechanics: Transport in Microfluidic Devices. Cambridge: Cambridge University Press; 2010

[2] Pethig RR. Dielectrophoresis: Theory, Methodology and Biological Applications. New Jersey, USA: John Wiley & Sons, Ltd; 2017

[3] Electrokinetics and Electrohydrodynamics in Microsystems. Wien: Springer-Verlag; 2011

[4] Chan KL, Morgan H, Morgan E, Cameron IT, Thomas MR. Measurements of the dielectric properties of peripheral blood mononuclear cells and trophoblast cells using AC electrokinetic techniques. Biochimica et Biophysica Acta (BBA) - Molecular Basis of Disease. 2000;**1500**: 313-322

[5] Koji A, Tetsuya H, Naokazu K. Dielectric approach to suspensions of ellipsoidal particles covered with a shell in particular reference to biological cells. Japanese Journal of Applied Physics. 1980; **19**:359

[6] Mansor M, Ahmad M. Single cell electrical characterization techniques. International Journal of Molecular Sciences. 2015;**16**:12686

[7] Adekanmbi E, Srivastava S. Dielectrophoretic applications for disease diagnostics using lab-on-a-chip platform. Lab on a Chip. 2016:2148

[8] Jubery T, Srivastava SK, Dutta P. Dielectrophoresis separation of bioparticles in microdevices: A review. Electrophoresis. 2014;**35**:691-713

[9] Irimajiri A, Hanai T, Inouye A. A dielectric theory of "multi-stratified shell" model with its application to a lymphoma cell. Journal of Theoretical Biology. 1979;**78**:251-269

[10] Di Biasio A, Ambrosone L, Cametti C. Dielectric properties of biological cells in the dipolar approximation for the single-shell ellipsoidal model: The effect of localized surface charge distributions at the membrane interface. Physical Review. E, Statistical, Nonlinear, and Soft Matter Physics. 2010;**82**:041916

[11] Gascoyne P, Pethig R, Satayavivad J, Becker FF, Ruchirawat M. Dielectrophoretic detection of changes in erythrocyte membranes following malarial infection. Biochimica et Biophysica Acta (BBA) - Biomembranes. 1997;**1323**:240-252

[12] Khoshmanesh K, Nahavandi S, Baratchi S, Mitchell A, Kalantar-zadeh K. Dielectrophoretic platforms for bio-microfluidic systems. Biosensors and Bioelectronics. 2011;**26**:1800-1814

[13] Gascoyne PR, Shim S. Isolation of circulating tumor cells by dielectrophoresis. Cancers (Basel). 2014;**6**:545-579

[14] Srivastava S, Gencoglu A, Minerick A. DC insulator dielectrophoretic applications in microdevice technology: A review. Analytical and Bioanalytical Chemistry. 2011;**399**:301-321

[15] Griffiths D. Introduction to Electrodynamics. 5th ed. Prentice Hall; 1999

[16] Neculae A, Bunoiu OM, Lungu M. Numerical simulation of bioparticle manipulation using dielectrophoresis. AIP Conference Proceedings. 2010; **1262**:144-149

[17] Mack C. 2006. Available from: http://lithoguru.com/scientist/publish.html

[18] Adekanmbi EO, Ueti MW, Rinaldi B, Suarez CE, Srivastava SK. Insulator-based dielectrophoretic diagnostic tool for babesiosis. Biomicrofluidics. 2016; **10**:033108

Edited by Ruby Srivastava

Biomimetic devices are designed and produced by materials, structures, and systems that are modelled on biological entities and processes. These devices are used to synthesize novel materials and their functions at the multiscale level for various applications. Molecular computing biological devices play a key role in the logical processing of the cellular machinery of all living organisms. This book includes information on both biomedical and technological applications of bioactive devices for hard tissue regeneration; design of chip-based disease diagnostic platforms; neuromorphic computing biomaterials that transfer techniques of neuroscience to a silicon chip; various top-down and bottom-up designs; and electrical characterization and transport mechanisms of DNA as nanowires.

IntechOpen